Shear heating of a fluid-saturated slip-weakening dilatant fault zone: 2. Quasi-drained regime

Dmitry I. Garagash
Department of Civil and Environmental Engineering, Clarkson University, Potsdam, New York, USA

John W. Rudnicki
Department of Civil and Environmental Engineering, Northwestern University, Evanston, Illinois, USA

Received 23 September 2002; revised 2 May 2003; accepted 1 July 2003; published 16 October 2003.

[1] This paper analyzes slip on a fluid-infiltrated dilatant fault for imposed (tectonic) strain rates much slower than the rate of fluid exchange between the gouge zone and the surroundings and for exchange of heat slower than of fluid, typical of interseismic or most laboratory loading conditions. The limiting solution, corresponding to the infinitely rapid drainage rate, developed in the companion paper by *Garagash and Rudnicki* [2003], yielded unbounded slip acceleration for sufficiently large slip weakening of the fault. Analysis for rapid but finite drainage rates (quasi-drained condition) reveals two types of possible instability. The first is inertial instability (a seismic event) characterized by an unbounded slip rate and attributed to the destabilizing effects of shear heating and fault slip weakening. The second corresponds to loss of uniqueness and arises from the small pressure increase caused by shear heating for rapid but finite rates of drainage. This instability emerges for even small amounts of thermomechanical coupling and a large range of dilatancy and slip weakening. Its resolution probably requires a more elaborate frictional description (e.g., rate and state), but within the slip-weakening framework here, leads to either slip arrest or inertial instability. The response is always unstable (in one of these two ways) for sufficiently large thermal coupling or initial stress regardless of the amount of slip weakening and dilatancy. The counterintuitive stabilizing effect of increased slip weakening or decreased dilatancy, similar to the effect in the companion paper, also occurs for nearly drained slip. *INDEX TERMS:* 3210 Mathematical Geophysics: Modeling; 3299 Mathematical Geophysics: General or miscellaneous; 5104 Physical Properties of Rocks: Fracture and flow; 5134 Physical Properties of Rocks: Thermal properties; 7209 Seismology: Earthquake dynamics and mechanics; *KEYWORDS:* shear heating, friction, dilatancy, slip-weakening, earthquakes, permeability

Citation: Garagash, D. I., and J. W. Rudnicki, Shear heating of a fluid-saturated slip-weakening dilatant fault zone: 2. Quasi-drained regime, *J. Geophys. Res.*, *108*(B10), 2472, doi:10.1029/2002JB002218, 2003.

1. Introduction

[2] Frictional slip or inelastic shear deformation in a fault zone generates heat and, if the heat does not escape sufficiently rapidly, can cause the temperature of an infiltrating pore fluid to increase. If the pore fluid is confined to the fault zone, the increase in temperature causes an increase in pore pressure, decreasing the effective compressive stress and, hence, the resistance to slip or inelastic shear deformation. Dilation, an inelastic increase in pore volume due to shear deformation or slip, tends to reduce the pore pressure and counteract an increase due to heating. The magnitude of these effects and their interaction depend on the relative rates of fault zone deformation and of the flux of fluid or heat from the fault zone.

0148-0227/03/2002JB002218$09.00

[3] Studies examining the role of shear heating [e.g., *Lachenbruch*, 1980; *Raleigh and Evernden*, 1981; *Mase and Smith*, 1987] have assumed steady slip or focused on its role during dynamic (seismic) slip [e.g., *Andrews*, 2002]. Shear heating can also affect whether slip is stable (aseismic) or unstable (seismic) [e.g., *Shaw*, 1995; *Sleep*, 1995] and, if unstable, the conditions at onset. Because shear heating depends on the absolute level of stress (not just its change), it introduces a depth dependence into the response in addition to that caused by depth variation of material and transport properties. Hence shear heating can affect the depth at which unstable slip initiate.

[4] This paper continues the investigation by *Garagash and Rudnicki* [2003] (hereinafter referred to as GR) of the role of shear heating on the stability of slip. In particular, they extended the saturated, slip-weakening, dilatant fault model by *Rudnicki and Chen* [1988](hereinafter referred to as RC) to include the effect of shear heating. The model is essentially a spring-slider system with fluid and heat flow

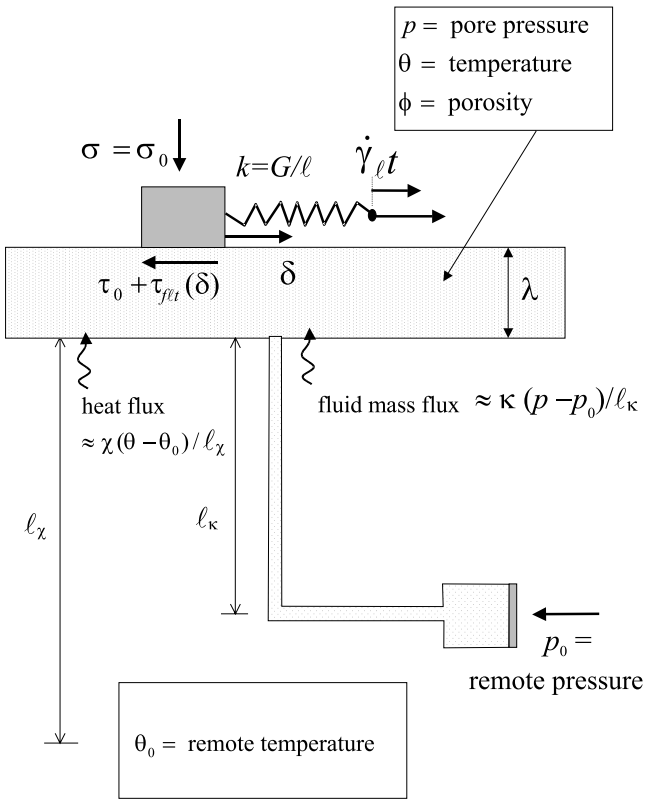

Figure 1. Model represented as a single-degree-of-freedom system.

from the fault zone assumed to be proportional to the difference of the pore pressure and temperature in the fault zone and remote values in the surrounding rock mass (Figure 1). This simple model, despite its limitations, has proven to be useful in assessing the roles of various physical processes, in delimiting the ranges of material and transport properties where different types of behavior may be expected, and in establishing a basis for understanding more realistic, but more complex models. In particular, the spring slider model has been widely used for the exploration of rate- and state-dependent constitutive models [e.g., *Rice and Ruina*, 1983; *Rice and Tse*, 1986; *Gu et al.*, 1984; *Blanpied and Tullis*, 1986; *Segall and Rice*, 1995; *Ranjith and Rice*, 1999; *Chambon and Rudnicki*, 2001].

[5] GR discussed estimates for the physical and normalized parameters of the problem for typical in situ conditions and studied the stability of slip in certain limiting regimes suggested by these estimates. These included the case of no dilation and no slip weakening, the fully drained case, in which fluid flow from the fault zone occurs much more rapidly than the slip rate, and the undrained, adiabatic case, in which no heat or fluid mass exchange occurs between the fault zone and the surroundings. The last is appropriate if the slip rate is large (compared with rates of fluid and heat exchange) as occurs as instability is approached. The undrained, adiabatic case is also appropriate if the fault is thermally and hydraulically sealed, as is likely to occur for at least some faults in situ.

[6] Unless the fault is hydraulically sealed, or nearly so, the rate of fluid exchange between the fault and the surrounding crust will be so much larger than the rate of loading by tectonic straining in the Earth's crust (or in typical laboratory conditions) that the fully drained approximation must apply for most of the slip history. For sufficient slip weakening, this approximation predicts the occurrence of an inertial instability corresponding to a seismic event [*Garagash and Rudnicki*, 2003; *Rudnicki and Chen*, 1988]. As the slip rate increases toward this instability, the fully drained approximation breaks down: slip is occurring more rapidly than fluid or heat can exchange with the surroundings. Neglecting the effect of shear heating, RC showed that dilation accompanying rapid slip can prevent this instability: rapid dilation reduces the pore fluid pressure, increases the effective compressive stress and, thus, the resistance to slip. Our goal in this paper is to determine how these conditions are altered by including shear heating.

[7] Because of thermal expansion, shear heating tends to increase the pore pressure of a confined fluid and, thus, would be expected to compete with the stabilizing reductions of pore fluid caused by dilatancy. The limiting cases in GR show, however, that pressure increases due to shear heating can be self-limiting: the pressure increase reduces the effective compressive stress and, thus, the magnitude of shear heating. Furthermore, examination of the undrained, adiabatic case demonstrated that dilatancy can actually contribute to destabilization by increasing the effective compressive stress and, thus, the rate of shear heating. In order to determine whether inertial slip instability does, in fact, take place under low rates of imposed straining (typical of most tectonic or laboratory conditions), it is necessary to relax the assumption of fully drained conditions and consider rapid, but finite drainage rates.

[8] Parameter ranges representative of field conditions are discussed in detail in GR. Although plausible ranges can be identified, estimates can vary over one, or even more, orders of magnitude due to uncertainty or variations in field conditions. As a result, we will consider a broad range of parameters and determine those ranges for which the response is predicted to be stable or unstable.

2. Formulation

[9] The formulation of the model is described in detail in GR but is briefly recapitulated here. The model is developed in GR for the layer geometry shown in their Figure 1 but is equivalent to the one degree-of-freedom, spring-slider system shown in Figure 1. The notation is described in the notation section. The response of the system is governed by three equations expressing equilibrium, fluid mass conservation, and energy conservation.

[10] Equilibrium of the slider requires that

$$\tau_o + G(\dot{\gamma}_\ell t - \delta/\ell) = \tau_o + \tau_{flt}(\delta) - \mu_o[p - p_o], \qquad (1)$$

where the left-hand side is the force in the spring, the right-hand side is the frictional resistance to sliding of the block (both expressed for a block of unit area), and τ_o is the initial shear stress when the time t and block slip δ are zero. The imposed rate of strain $\dot{\gamma}_\ell$ is taken to be representative of tectonic strain rates, G is the shear modulus of the material surrounding the fault and ℓ is a characteristic length of the crustal block. The second term on the right-hand side $\tau_{flt}(\delta)$

is the dependence of the fault frictional resistance on slip (at constant effective compressive stress). As discussed in more detail in GR, the dependence is assumed to be simply on the slip rather than on the rate of slip and the state of the frictional surface. The last term on the right-hand side is the product of a friction coefficient μ_o and the change in the effective compressive stress. The effective compressive stress is the difference between the total compressive stress and the pore pressure, but because the total compressive stress is assumed to be constant (and the initial value is absorbed into τ_o), only the difference between the fault zone pore pressure p and the remote, ambient value p_o appears in equation (1).

[11] Fluid mass conservation is expressed as

$$\lambda_o\left\{\frac{d\phi^p}{d\delta}\dot{\delta}+\frac{\dot{p}}{K'}-\beta'\dot{\theta}\right\}=-\kappa\frac{p-p_o}{\ell_\kappa}, \tag{2}$$

where the left-hand side is the rate of change of fluid mass in the fault zone and the right-hand side is fluid flux into the fault zone. As in RC and *Segall and Rice* [1995], fluid mass flux from the fault zone is assumed to be proportional to the difference between the pore pressure in the fault p and a remote pore pressure p_o, and divided by a characteristic length ℓ_κ over which diffusion occurs; κ is fluid conductivity. The initial thickness of the fault zone is λ_o. The three terms on the left-hand side are the fluid mass change due to change of inelastic porosity ϕ^p (assumed to be a function only of the slip δ), the change of pore pressure, $\dot{p}$, and the change of temperature, $\dot{\theta}$, respectively. The coefficients K' and β' are the effective bulk modulus and thermal expansivity, respectively.

[12] Energy conservation is expressed as

$$\lambda_o C\dot{\theta}=\tau\dot{\delta}-\chi\frac{\theta-\theta_o}{\ell_\chi}, \tag{3}$$

where the heat flux, the second term on the right-hand side is modeled in a manner similar to fluid diffusion: ℓ_χ is a characteristic length and χ is a thermal conductivity. The first term on the right-hand side is the rate of heating caused by frictional slip with τ given by either the right or left-hand side of equation (1). The left-hand side of equation (3) is the rate of heat change in the fault zone with C denoting the heat capacity.

[13] Equations (1), (2), and (3) comprise a complete system, but it is useful to combine them to yield

$$\left\{\frac{G}{\ell}+\frac{d\tau_{flt}}{d\delta}-\mu_o K'\left[\frac{\beta'\tau}{\lambda_o C}-\frac{d\phi^p}{d\delta}\right]\right\}\dot{\delta}=G\dot{\gamma}_\ell-\frac{\mu_o}{t_\kappa}(p-p_o)-\frac{\mu_o K'\beta'}{t_\chi}(\theta-\theta_o), \tag{4}$$

where $t_\kappa=\lambda_o\ell_\kappa/\kappa K'$ and $t_\chi=\lambda_o\ell_\chi C/\chi$ are timescales of pore fluid and thermal diffusion, respectively. The system of equations governing the response is now equation (4) (which is identical to equation (16) of GR), (3) and (1).

[14] The variation of the fault shear stress τ_{flt} is taken to have the same simple forms as in RC (discussed in more detail there and in GR):

$$\tau_{flt}=-(\tau_o-\tau_r)g(\delta/\delta_r), \tag{5}$$

where $\tau_r<\tau_o$ and

$$g(x)=\begin{cases}-2x^3+3x^2 & 0\le x\le 1\\ 1 & x>1.\end{cases} \tag{6}$$

Similarly, the inelastic porosity ϕ^p is taken to have the form

$$\phi^p=\phi^p_r f(\delta/\delta_r), \tag{7}$$

where

$$f(x)=\begin{cases}2x-x^2 & 0\le x\le 1\\ 1 & x>1.\end{cases} \tag{8}$$

(Because RC do not include the initial fault zone thickness, denoted here by λ_o, in their formulation, the function f is used for the fault opening (relative normal displacement) rather than the inelastic porosity.) Writing equations (4), (3), and (1) in nondimensional form in terms of normalized time T, slip Δ, and temperature Θ (see notation section for definitions) yields

$$\dot{\Delta}=\frac{1}{\epsilon}\frac{N(\Pi,\Theta)}{D(T,\Delta)} \tag{9a}$$

$$\dot{\Theta}=\Sigma_\tau\dot{\Delta}-\frac{1}{\epsilon_\chi}\Theta. \tag{9b}$$

The numerator N and denominator D in equation (9a) are

$$N=-\Pi+\epsilon\left(1-\frac{\mathcal{B}}{\epsilon_\chi}\Theta\right) \tag{10}$$

$$D=\Phi f'(\Delta)+1-\frac{2}{3}\mathcal{A}g'(\Delta)-\mathcal{B}\Sigma_\tau, \tag{11}$$

and the dimensionless pressure Π and shear stress Σ_τ are given by

$$\Pi=-T+\Delta-\frac{2}{3}\mathcal{A}g(\Delta) \tag{12a}$$

$$\Sigma_\tau=\Sigma^o_\tau+\mu_o(T-\Delta). \tag{12b}$$

[15] The nondimensional equations contain two ratios of timescales, $\epsilon=t_\kappa/(\delta_r/\dot{\gamma}_\ell\ell)$ and $\epsilon_\chi=t_\chi/(\delta_r/\dot{\gamma}_\ell\ell)$, a stress state parameter, Σ^o_τ, and three material parameters $\mathcal{A}$, $\mathcal{B}$, and Φ, expressing the magnitudes of slip weakening, thermal expansion, and dilatancy, respectively. Representative values of these parameters for in situ conditions are discussed in detail by GR. Both ϵ and ϵ_χ are very small with ϵ_χ ranging from 10^{-6} to 10^{-2} and ϵ a factor of 10^{-4} smaller. $\mathcal{A}$ is generally of the order of unity, in the range 0.1–10, and representative values of Φ range from 0.004 to 4.0. The parameter $\mathcal{B}$ is depth-dependent, reflecting depth dependence of the coefficient of thermal expansion. It increases

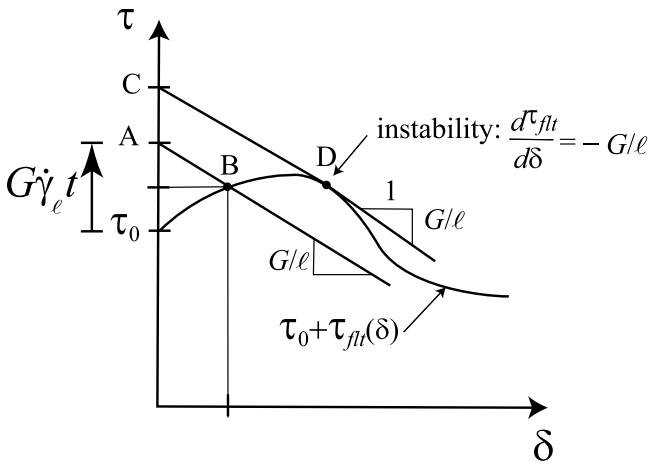

Figure 2. Graphical illustration of the response in the limit of drained deformation, $p = p_o$.

roughly linearly for depths greater than 3 km and by less than a factor of 2 between 3 and 8 km. At 8 km depth, GR estimate that $\mathcal{B}$ is in the range 0.0034–0.34. The stress state parameter Σ_τ^o is equal to the ratio of the initial stress τ_o, assumed to be the peak value, to a characteristic pressure $p_* = G\delta_r/\mu_0\ell$. GR estimate p_* as 0.5–5.0 MPa and, for a lithostatic stress gradient (30 MPa km^{-1}), a hydrostatic pore pressure gradient (10 MPa m^{-1}), and a depth-independent frictional stress reduction of $\tau_o - \tau_r \approx 10$ MPa, $\tau_o = 10 + 12\times$ (depth in km). The relatively large ranges of values of these parameters are due to both uncertainty about in situ values of material and transport properties and about the appropriate value of the length ℓ in the spring-slider system needed to simulate the more complex actual system.

3. Limiting Cases

[16] GR analyzed a number of limiting cases that illustrate the effects of shear heating and, in addition, accurately describe the response of the system over a portion of its history. A brief recapitulation of some of these cases will be useful as an introduction to the following analysis and to aid in interpretation of the results.

[17] The physical interpretation of the small value of ϵ (10^{-10} to 10^{-6}) is that the timescale of imposed tectonic straining is very much longer than that for fluid mass transfer between the fault zone and the surrounding crust. Consequently, during the long interseismic period, when the fault shear strain rate is of the same order as the tectonic rate, any alterations of pore pressure due to dilation or shear heating are alleviated by fluid mass transfer (at least if the fault zone is not sealed). Thus the response is well approximated by equation (1) with $p = p_o$. The solution of this equation is illustrated by the graphical construction of *Rice* [1979] and shown in Figure 2.

[18] The solution for the current shear stress τ and the current slip δ is point B, the intersection of the straight line given by the left-hand side of equation (1) with the fault constitutive relation given by the right-hand side (with $p = p_o$). As the imposed far-field strain ($\dot{\gamma}_\ell t$) increases, point A moves upward and the intersection point B moves to the right, in the direction of increasing δ. If the shear stress on the fault decreases sufficiently rapidly (corresponding to values of the nondimensional slip-weakening parameter $\mathcal{A} > 1$), the solution cannot be continued past point D. The mathematical expression of this point is obtained by differentiating equation (1):

$$\left[\frac{G}{\ell} + \frac{d\tau_{\rm flt}(\delta)}{d\delta}\right]\dot{\delta} = G\dot{\gamma}_\ell. \tag{13}$$

At point D, the coefficient of $\dot{\delta}$ vanishes and the ratio of the increment of fault slip to remote displacement becomes unbounded indicating that the inertial terms neglected in the equilibrium equation for the block need to be included. Because the rate of fault slip $\dot{\delta}$ increases as point D is approached, the underlying assumption that the slip rate is much slower than the rate of fluid mass exchange breaks down in the vicinity of this point. The more elaborate solution needed to correct this breakdown is the primary subject of this paper.

[19] The alternative limiting case of adiabatic and undrained response, for which the fault exchanges no fluid or heat with the surroundings, is also relevant to the analysis here. As the system approaches instability (such as that at point D in Figure 2), the fault slip rate will become too large to allow time for significant transfer of heat and fluid between the fault zone and the surrounding material. In addition, the adiabatic, undrained solution is appropriate if the fault zone is hydraulically and thermally sealed. Several authors [*Sibson*, 1973; *Lachenbruch*, 1980; *Byerlee*, 1990] have suggested that faults are hydraulically sealed.

[20] The undrained, adiabatic limit corresponds to omitting the last two terms on the right-hand side of equation (4) or, in terms of nondimensional parameters, letting $\epsilon, \epsilon_\chi \to \infty$. The graphical construction shown in Figure 3 illustrates the solution. The effective τ versus δ curve differs from the drained curve because of the alteration of pore pressure by shear heating and dilation. Thus the difference between the undrained, adiabatic curve and the drained curve is the last term in equation (1). Figure 3 depicts a case where an inertial instability, like that at point D in Figure 2, occurs

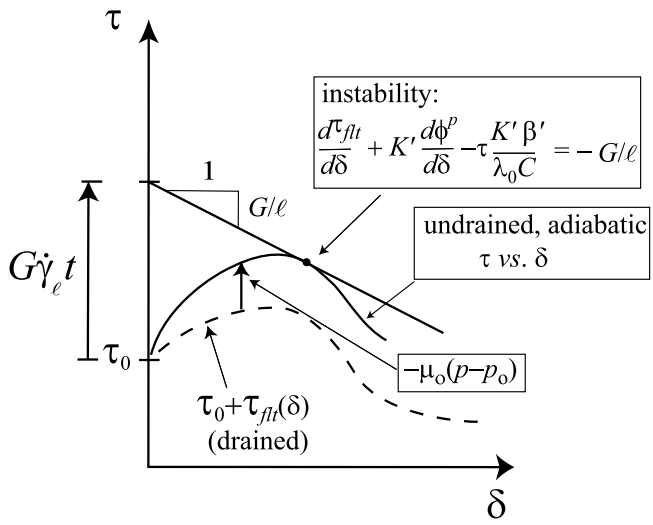

Figure 3. Graphical illustration of the undrained, adiabatic solution.

because the slope of the τ versus δ curve falls to $-G/\ell$. However, as discussed in detail by GR, whether instability occurs depends on the relative contributions of dilation and shear heating. For dilation, $d\phi^p/d\delta > 0$, the coefficient of $\dot{\delta}$ on the left-hand side of equation (4) tends to increase the slope of the τ versus δ curve. Conversely, the preceding term in equation (4), due to shear heating, tends to decrease the slope. A complicating effect is, however, due to the dependence of the shear heating on τ, which is equal to either side of equation (1) and depends on the pore pressure. Shear heating tends to increase the pore pressure, but this, in turn, decreases the value of τ and the rate of shear heating. Conversely, dilation tends to reduce the pore pressure, but this increases τ and the rate of shear heating. The numerical examples and analysis in GR demonstrate that this interdependence can cause increased slip weakening to be stabilizing and increased dilation to be destabilizing.

4. Quasi-Drained Solution

[21] As noted in section 3, the timescale of imposed straining is very much longer than that for fluid mass flux from the fault zone for fault systems, as well as for most laboratory conditions and, consequently, $\epsilon \ll 1$. Because ϵ is so small, in the range 10^{-6} to 10^{-10} (GR), the slip rate is slow enough that (nearly) fully drained conditions prevail during most of the slip history. Mathematically, this means that as long as the dimensionless slip rate remains bounded, $\dot{\Delta} \ll 1/\epsilon$, the small parameter ϵ can be taken to zero. This limit yields the fully drained ($\epsilon = 0$) slip solution $T = T_d(\Delta)$, $\Pi = 0$, and $\Theta = \Theta_d(\Delta)$ (see RC for the thermo-uncoupled case and section 5.2 of GR). If the weakening parameter is small enough, $\mathcal{A} < 1$, this solution provides a good approximation to the entire slip history. If, however, $\mathcal{A} \geq 1$, the fully drained solution yields an unbounded slip rate at critical values of the nondimensional time T_* and slip Δ_* (see Figure 2 and Figure 4a of GR). The occurrence of this unbounded slip rate violates the condition that $\dot{\Delta} \ll 1/\epsilon$ and the underlying assumption of full drainage. Therefore the rate of pore pressure change cannot be neglected for (nondimensional) time and slip values in the vicinity of T_* and Δ_*, respectively. A more refined asymptotic analysis of the full slip equations is needed for small but nonzero values of the drainage parameter ϵ. In particular, the refined analysis is necessary to determine whether slip instability does indeed occur under these conditions or, perhaps, is stabilized by rapid dilation, as in the case of the thermally uncoupled analysis (RC).

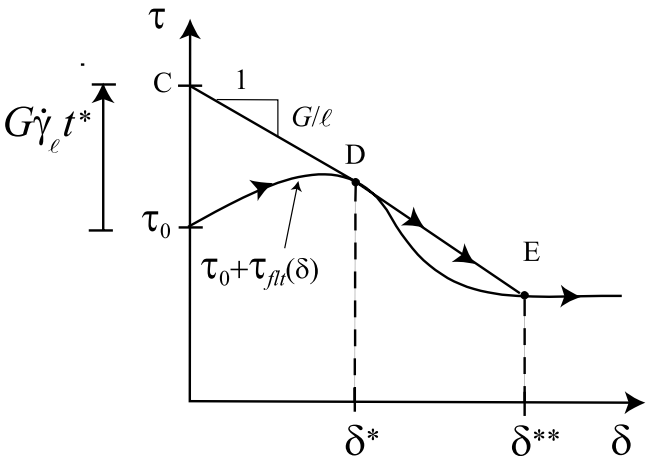

Figure 4. Graphical illustration of the quasi-drained asymptotic slip solution (15).

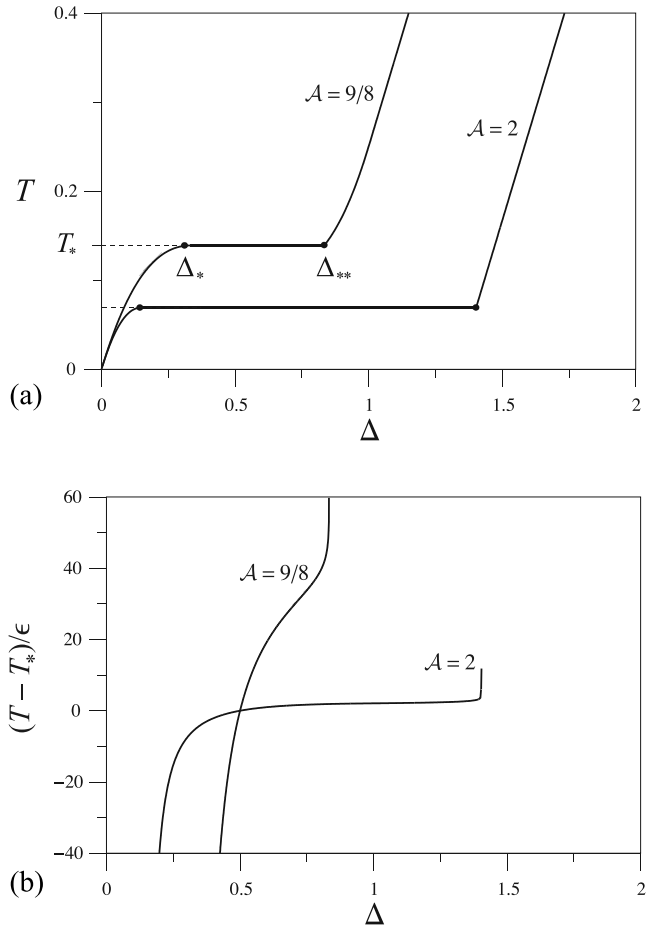

Figure 5. Quasi-drained solution for two values of fault weakening $\mathcal{A} = \{9/8, 2\}$ and the other parameters fixed ($\mathcal{B} = 0.075$, $\Phi = 5$, $\Sigma_\tau^o = 10$, $\mu_o = 0.6$, and $\epsilon_\chi = 0.01$) for (a) time T versus slip Δ (bounds of the fast slip regime (thick lines) are indicated by dots) and (b) "rapid" time $\xi = (T - T_*)/\epsilon$ versus slip Δ in the fast slip regime.

[22] The asymptotic analysis for $\mathcal{A} \geq 1$ expands the similar analysis of RC for the thermally uncoupled slip, and, consequently, is omitted here for brevity. The result, termed the quasi-drained solution, consists of the three primary consecutive slip regimes. The equations describing these regimes are given in the Appendix A.

[23] Essentially, the quasi-drained slip solution corresponds to the fully drained solution ($\epsilon = 0$) but with the nonphysical portion of the T versus Δ curve replaced by a stretch of fast slip, $T \simeq T_*$. As described in GR, the nonphysical portion of the drained T versus Δ curve occurs where Δ increases with decreasing T (see, e.g., the dashed dip in the curve in Figure 4a of GR for $\mathcal{A} = 9/8$). The three primary slip regimes are connected by the transitional regimes of order ϵ in both T and Δ. Physically, the three regimes correspond to the very slow slip rate under drained

conditions that characterizes the interseismic period, a rapid slip regime, and a return to slow slip under drained conditions.

[24] Figure 4 gives a graphical illustration of this solution. The solution is equal (to order ϵ) to the fully drained solution (given by equation (1) with $p = p_o$) until point D at time t_* (nondimensional time T_*) and slip δ_* (nondimensional slip Δ_*). At point D instability would occur in the fully drained solution. Instead, the asymptotic solution follows the line DE between slip values δ_* and δ_{**} (nondimensional values Δ_* and Δ_{**}). During slip from δ_* to δ_{**}, the pore pressure change (times μ_o) is equal to the difference between DE and the curve $\tau_o + \tau_{flt}(\delta)$ and thus is given by equation (1) with $t = t_*$:

$$\mu_o[p - p_o] = -\{G(\dot{\gamma}_\ell t_* - \delta/\ell) - \tau_{flt}(\delta)\}. \qquad (14)$$

[25] Figures 5 and 6 show the quasi-drained solutions for two values of fault weakening parameter $\mathcal{A} = \{9/8, 2\}$ and fixed $\mathcal{B} = 0.075$, $\Phi = 5$, $\Sigma_\tau^o = 10$, $\mu_o = 0.6$, and $\epsilon_\chi = 0.01$. The critical time T_* and the slip values delineating the fast slip regime, Δ_* and Δ_{**} (as indicated in Figure 5a for the $\mathcal{A} = 9/8$ case), are functions of $\mathcal{A}$ only (see equations (A2)–(A4) of GR for explicit expressions). Initially, fully drained slip accelerates and gives way to the fast slip at $T \simeq T_*$ at which time the drained approximation does not apply. After sliding the distance $\Delta_{**} - \Delta_*$ in the fast slip regime, slip decelerates and returns to the drained (slow) regime. When the slip is stable, the mechanical part of the solution (slip and pressure) is the same (to the order ϵ) as in the solution of the thermo-uncoupled case considered by RC. In the fast slip regime, the thermomechanical coupling significantly alters the slip evolution (Figure 5b).

[26] Figure 5b rescales the time axis to show the details of slip evolution near T_*. For $\dot{\gamma}_\ell = 10^{-15}$ s^{-1} and $\delta_r = 0.1$ m, a nondimensional time $T = 1$ corresponds to 32×10^3 years for $\ell = 10^2$ m or 3200 years for $\ell = 10^3$ m. For $\epsilon = 10^{-6}$, one unit of the "rapid time," $\xi = (T - T_*)/\epsilon$, corresponds to 11.6 days or 1.16 days for the two values of ℓ. Values decrease in proportion to ϵ. Although the (nondimensional) slip rate $d\Delta/dT$ appears to be extremely high in Figure 5, even in the expanded scale for $\mathcal{A} = 2.0$, it remains several orders of magnitude less than seismic rates. For a tectonic shear rate of $\dot{\gamma}_\ell \sim 10^{-15}$ s^{-1} and a crustal block of length $\ell \sim 10^3$ m, the characteristic tectonic slip rate on the fault $\ell\dot{\gamma}_\ell$ is about 10^{-12} m s^{-1}. In order for the dimensional slip rate on the fault, $d\delta/dt = (\ell\dot{\gamma}_\ell)\,(d\Delta/dT)$, to reach a representative seismic magnitude of 1 m s^{-1}, the dimensionless slip rate $d\Delta/dT$ must be about 10^{12}. Typically, the nondimensional slip rate is of the order of ϵ^{-1} in the fast slip regime (where ϵ ranges from 10^{-10} to 10^{-6}). Consequently, for this estimate, the slip rate in the fast slip regime is at least 2 orders of magnitude smaller than the seismic rate.

[27] Figures 6a and 6b show the changes in pressure and temperature, respectively. The combined effects of fault dilatancy and weakening cause the pore fluid pressure to drop and the magnitude of the drop increases with the fault weakening $\mathcal{A}$. (Recall that in the fully drained regimes the pressure is equal, to the order ϵ, to its ambient constant value, $\Pi = 0$.) For a value of the characteristic pressure p_* of 5–10 MPa (GR), the maximum nondimensional pressure change of $\Pi \sim 0.5$ ($\mathcal{A} = 2$ in Figure 6a) corresponds to a pressure drop of 2.5 to 5.0 MPa. These values are 3 to 6% of the ambient pressure at 8 km depth assuming a hydrostatic pressure gradient (10 MPa km^{-1}).

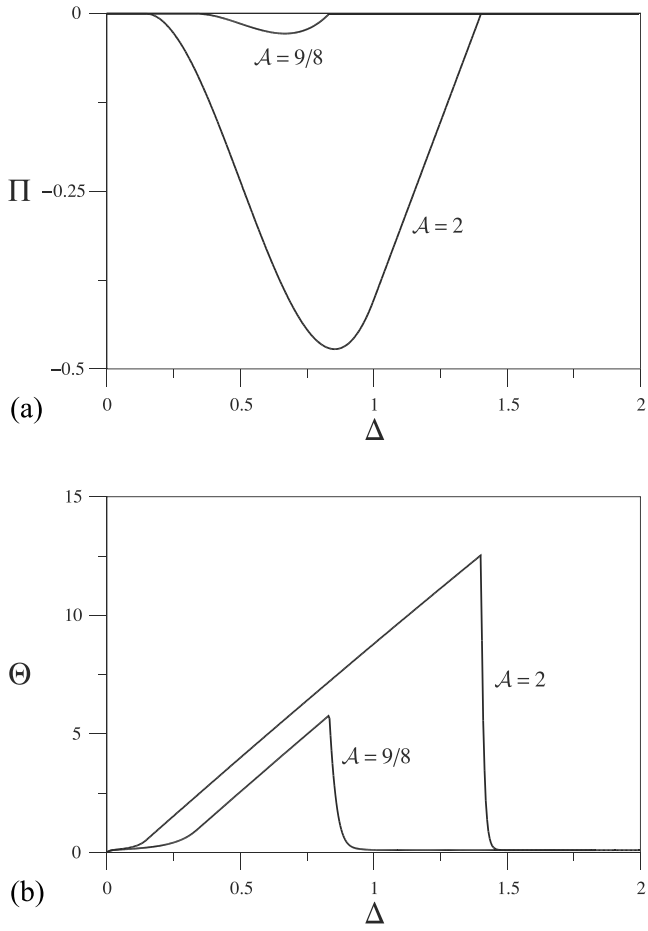

Figure 6. Quasi-drained solution (Figure 5) for (a) pressure Π and (b) temperature Θ versus slip Δ.

[28] The temperature rises almost linearly in the fully drained regime of accelerating slip and in the fast slip regime (Figure 6b) and then drops abruptly as slip decelerates exponentially at the end of the fast slip regime. At large times in the later fully drained regime, the temperature (equation (A6)) approaches a steady state constant value $\epsilon_\chi \Sigma_\tau^r$, where $\Sigma_\tau^r = \Sigma_\tau^o - \frac{2}{3}\mu_o \mathcal{A}$ is the residual shear stress and ϵ_χ^{-1} is the normalized thermal conduction. For values of the characteristic temperature θ^* ranging from 0.17 to 17°C, the maximum temperature rise for $\mathcal{A} = 9/8$ is 0.85–85°C. For $\mathcal{A} = 2.0$, the values range from 2.0 to 204°C. The large range of possible values reflects uncertainty about the fault zone thickness ($\lambda_o = 10^{-2}$ to 1 m) assuming a fixed volumetric heat capacity of $C = 3$ Mpa °C $^{-1}$ (GR). The larger values are significant fractions of the ambient temperature at 8 km depth assuming a thermal gradient of 20–25°C km [*Henyey and Wasserburg*, 1971; *Lachenbruch and Sass*, 1973; GR], demonstrating that shear heating can cause a significant temperature rise even when slip is not dynamic.

[29] The dependence of the solution in the fast slip regime on thermomechanical coupling parameter $\mathcal{B}$ is illustrated in Figure 7. The dashed lines show the fast slip asymptotic solutions for the scaled slip rate, $\epsilon d\Delta/dT$ (or $d\Delta/d\xi$ in terms of the "rapid" time ξ), versus slip for various values of $\mathcal{B}$,

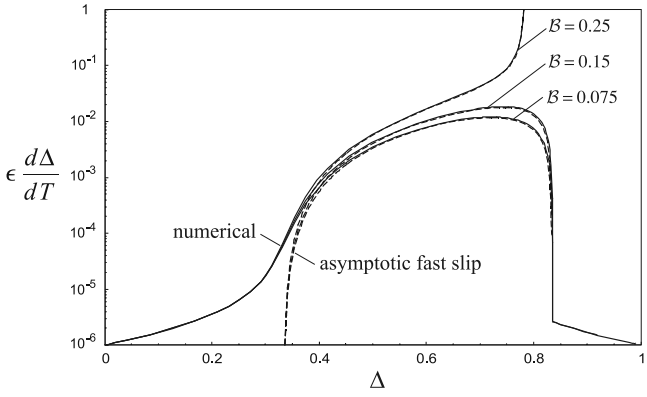

Figure 7. Slip rate with respect to the "rapid" time, $\epsilon d\Delta/dT$ (or $d\Delta/d\xi$) versus slip Δ for three values of thermomechanical coupling $\mathcal{B}$, fixed $\epsilon = 10^{-6}$, $\mathcal{A} = 9/8$, and the rest of parameters as in Figures 5 and 6. Dashed lines correspond to the asymptotic solution in the fast slip regime (see equation (A3)), and solid lines correspond to the numerical solution.

fixed $\mathcal{A} = 9/8$, and the other parameters as in Figures 5 and 6 (the vertical asymptotes correspond to the slip values Δ_* and Δ_{**}). For comparison, solutions of the general slip equations with $\epsilon = 10^{-6}$, obtained with a numerical ODE solver (Mathematica, version 4.1, copyright 1988–2000 Wolfram Research, Inc.), are shown by solid lines over the complete slip range. The numerical and asymptotic solutions were indistinguishable on plots such as Figures 5a and 6. The values chosen for $\mathcal{B}$ are within the range 0.34 to 0.0034 estimated by GR for 8 km depth. Again, the range primarily reflects uncertainty about the fault zone thickness. The depth dependence of $\mathcal{B}$ is mainly due to depth dependence of the pore fluid (assumed to be water) thermal expansion coefficient β_f. For depths greater than about 3 km, β_f increases approximately linearly from about 0.7×10^{-3} °C at 3 km to 1.1×10^{-3} °C at 8 km (see Figure 3 of GR).

[30] As shown on Figure 7, the maximum slip rate increases with an increase in $\mathcal{B}$ indicating the anticipated destabilizing effect of the shear heating. Eventually, for sufficiently large $\mathcal{B} = 0.25$, the solution becomes unstable. For undrained, adiabatic slip (section 5.3 of GR) and these same parameters, slip is unstable for values of $\mathcal{B}$ greater than about 0.084. In contrast to the thermally uncoupled response (RC), for which the undrained case gives a good indication of the occurrence of instability, this result suggests that the undrained, adiabatic case substantially underestimates the thermomechanical coupling $\mathcal{B}$ required to cause the instability.

5. Stability/ Uniqueness Analysis

[31] Section 4 illustrated the solution in the fast slip regime for both stable and unstable cases. The example shown in Figure 7 demonstrated the expected result that increased shear heating caused a dynamic instability. However, does increasing $\mathcal{B}$ always lead to an instability of this type for different values of the other parameters? When slip is unstable, how does the critical value of $\mathcal{B}$ depend on the other material properties? In principle, the answers to these and other questions could be obtained by systematic evaluation of the solution of section 4 for different sets of parameters. Unfortunately, even for the simple model used here, the wide ranges of material parameters make this a prodigious (not to mention inefficient) undertaking. Instead, in this section, we take advantage of the smallness of ϵ (and the simplicity of the model) to derive conditions for which the slip solution is stable or unstable for conditions of rapid drainage ($\epsilon \ll 1$). Furthermore, we show that when instability does occur, it can be one of two types.

[32] We first formally combine the fully drained ($\mathcal{A} < 1$) (equations (A1) and (A2)) and quasi-drained ($\mathcal{A} \geq 1$) (equations (A1)–(A6)) solutions to obtain the rapid drainage asymptotic slip solution

$$T_o(\Delta) = \begin{cases} T_d(\Delta), & 0 < \Delta \leq \Delta_*, \quad \Delta_{**} \leq \Delta < \infty \\ T_*, & \Delta_* \leq \Delta \leq \Delta_{**}. \end{cases} \tag{15}$$

This solution is valid to the order ϵ for the entire range of $\mathcal{A} \geq 0$. For $\mathcal{A} \geq 1$, equation (15) is identical to the quasi-drained solution characterized by the existence of the fast slip range, $\Delta_* \leq \Delta \leq \Delta_{**}$ with $\Delta_{**} \geq \Delta_*$; and for $\mathcal{A} < 1$, equation (15) reduces to the fully drained slip solution $T = T_d(\Delta)$ since the fast slip interval disappears, $\Delta_{**} - \Delta_* \to 0$, in the limit as $\mathcal{A}$ approaches one from above.

[33] The stability and uniqueness criteria are deduced by examining the nature of the differential equation governing the slip (equations (9a) and (9b)) and exploiting the nearness of the exact solution (within an order ϵ) to equation (15). The analysis is fully described in Appendix B and leads to the following conclusions:

[34] 1. Slip is stable (i.e., the slip rate is bounded and small perturbations about the solution decay) and given to the order ϵ by the asymptotic solution $T = T_o(\Delta)$ (equation (15)) if and only if the denominator in the slip equation (equation (11)) is positive, $D(T_o(\Delta), \Delta) > 0$, for all $\Delta \geq 0$. (This condition is formally identical to that for instability of undrained, adiabatic slip, but in that case, $D(T(\Delta), \Delta)$ is evaluated for the undrained, adiabatic slip solution $(T_u(\Delta), \Delta)$; see section 5.3 of GR.) In dimensional terms, the criterion for stable slip is

$$\frac{G}{\ell} + \frac{d\tau_{\text{flt}}}{d\delta} - \mu_o K' \left[\frac{\beta' \tau}{\lambda_o C} - \frac{d\phi^p}{d\delta} \right] > 0. \tag{16}$$

[35] 2. Slip is unstable when there exist values Δ_{ins}, such that

$$D(T_o(\Delta_{\text{ins}}), \Delta_{\text{ins}}) = 0. \tag{17}$$

Instability can occur in either of two ways: (1) In the fast slip regime ($\mathcal{A} > 1$), $\Delta_* \leq \Delta_{\text{ins}} \leq \Delta_{**}$, $D(T_*, \Delta_{\text{ins}}) = 0$ corresponds to an unbounded slip rate $\dot{\Delta} = \infty$; and (2) in a fully drained regime, $0 < \Delta_{\text{ins}} \leq \Delta_*$ or $\Delta_{**} \leq \Delta_{\text{ins}} < \infty$ with $D(T_d(\Delta_{\text{ins}}), \Delta_{\text{ins}}) = 0$, corresponds to the loss of solution uniqueness and sensitivity of the subsequent solution to small perturbations.

[36] Instability occurs in the fast slip regime when the denominator of equation (9a) vanishes (equation (17)) but

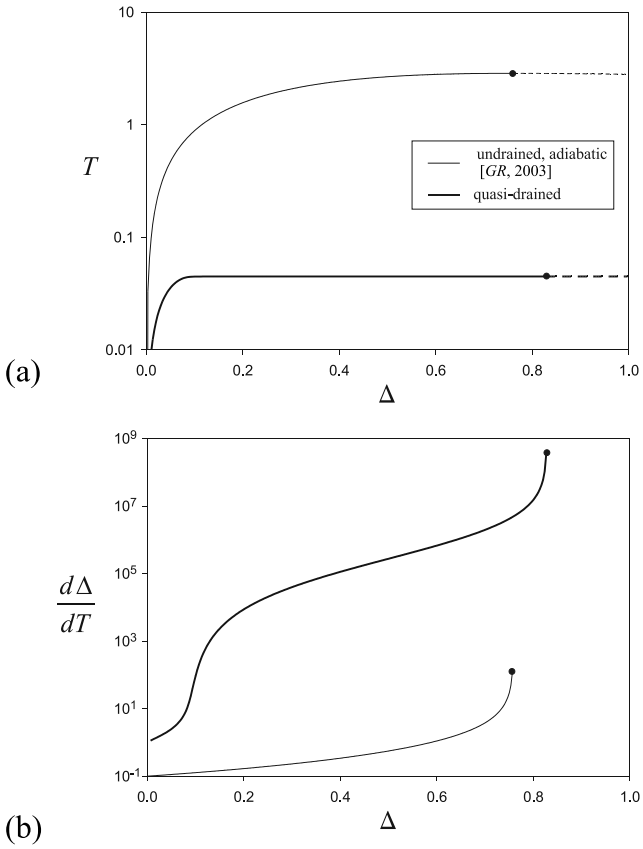

Figure 8. Illustration of inertial instability in the rapid drainage solution ($\epsilon = 10^{-6}$, $\epsilon_\chi = 10^{-2}$, thick lines) and undrained, adiabatic solution ($\epsilon = \epsilon_\chi = \infty$, thin lines) for (a) time T and (b) slip rate $d\Delta/dT$ versus slip Δ. ($\mathcal{A} = 3$, $\Phi = 5$, $\mathcal{B} = 0.1185$, $\Sigma_\tau^o = 9$, and $\mu_o = 0.6$). Physically meaningless parts of the slip after an instability are shown by dashed lines.)

the numerator remains positive. This is the same type of instability that occurs for the fully drained and fully undrained adiabatic responses. For both these limiting cases, the slip is governed by an equation with the right-hand side equal to $G\dot{\gamma}_\ell$, which is always positive. (For the drained case, the slip is governed by equation (13), and equation (4) reduces to $p = p_o$. For the undrained, adiabatic case, the last two terms on the right-hand side of equation (4) vanish because t_κ, $t_\chi \to \infty$ and equation (4) reduces to the same form as equation (13) with $d\tau_{flt}/d\delta$ replaced by the slope of the undrained, adiabatic τ versus δ curve.) The numerator of equation (9a), $N(\Pi, \Theta)$, corresponds in dimensional form to the right-hand side of equation (4). For finite ϵ, the response is neither fully drained nor undrained and adiabatic and the last two terms on the right-hand side do not vanish. However, for rapid slip (compared to timescales of fluid and heat exchange), these terms are small enough that the right-hand side of equation (4) is positive. Hence the instability is analogous to that in the drained and the undrained, adiabatic cases. In particular, instability is an inertial one with $\dot{\delta}$ and $\dot{\Delta}$ becoming unbounded corresponding to a seismic event and has a graphical expression similar to that in Figure 3, although the effective τ versus δ curve will differ from the undrained adiabatic one.

[37] Figure 8 shows a numerical example of the variation of time T and slip rate $d\Delta/dT$ with slip Δ in the rapid drainage case ($\epsilon = 10^{-6}$, $\epsilon_\chi = 10^{-2}$) for the inertial type of instability in the fast slip regime. (The corresponding undrained, adiabatic ($\epsilon = \epsilon_\chi = \infty$) solution (GR) is also shown by thin lines). The rapid drainage solution evolves to the inertial instability much faster (in time) than the undrained solution (Figure 8a) because of the period of fast slip with $d\Delta/dT \sim \epsilon^{-1} = 10^6$ (Figure 8b) prior to the instability. Figure 9 shows changes of the effective stress,

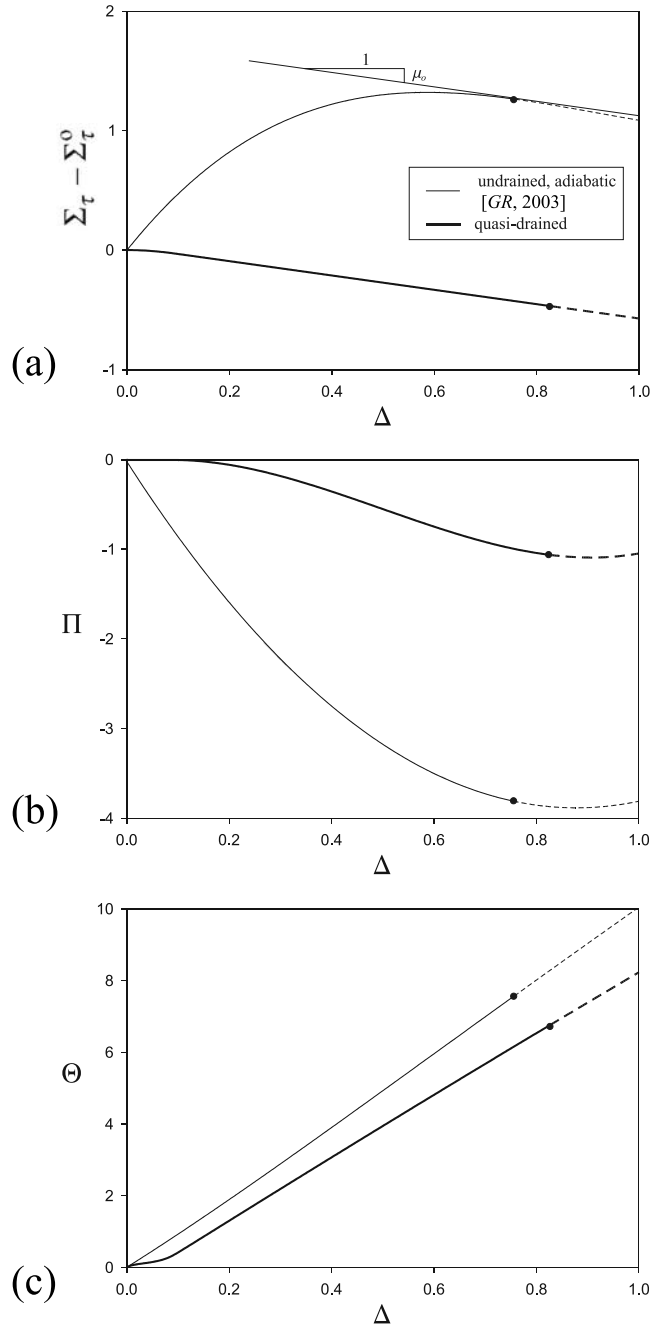

Figure 9. Illustration of inertial instability in the rapid drainage solution and undrained, adiabatic solution (Figure 8) for dimensionless variation of (a) shear stress, $\Sigma_\tau - \Sigma_\tau^o$, (b) pressure, Π, and (c) temperature, Θ, versus slip Δ.

$\Sigma_\tau - \Sigma_\tau^o$, pressure, Π, and temperature, Θ, with slip. As suggested by the preceding estimates, the pressure drop is large, indicating that dilation induced pressure reduction dominates heating induced increase and that the temperature rise, though significant, is not large enough to overcome the smallness of $1/t_\chi$ (see Figures 9b and 9c). The inertial instability in both rapid drainage and undrained solutions occurs because the slope of the dimensionless effective shear stress versus slip relation decreases to the value for elastic unloading (in dimensionless terms: $d\Sigma_\tau/d\Delta = -\mu_o$; see Figure 9a).

[38] Instability occurs in the slow slip (fully drained) regime when the denominator and the numerator in equation (9a) or, equivalently, the right-hand side and the coefficient of $\dot{\delta}$ in equation (4), vanish simultaneously. The absence of this type of instability in the drained and undrained, adiabatic cases suggests that it is due to the interaction of shear heating with fluid exchange between the fault and the surrounding material. Support for this suggestion can be obtained by examination of the right-hand side of equation (4). If, for simplicity, we assume adiabatic conditions ($t_\chi \to \infty$), the right-hand side of equation (4) can vanish only if the fault zone pressure exceeds the initial ambient value, $p > p_o$. (Since $t_\chi \gg t_\kappa$ ($\epsilon \ll \epsilon_\chi$), the assumption of adiabatic conditions is a good approximation and the neglect of the heat flux, last term on the right-hand side of equation (4), does not affect the argument here.) The equation governing the rate of pore pressure change is given by

$$\dot{p} = K'\left\{\frac{\beta'}{\lambda_o C}\tau - \frac{d\phi^p}{d\delta}\right\}\dot{\delta} - \frac{1}{t_\kappa}(p - p_o), \tag{18}$$

where, again, we have assumed adiabatic conditions. The pore pressure increases if the term due to shear heating, $\beta'\tau/\lambda_o C$ exceeds that due to dilation $d\phi^p/d\delta$. The effect of flow from the fault zone, the second term on the right-hand side, may diminish the rate of pore pressure change but will not reverse its sign. In terms of nondimensional parameters, $\{\ldots\}$ is initially positive (for $\tau = \tau_o$ and $f'(0) = 2$) if

$$\Phi < \mathcal{B}\Sigma_\tau^o/2. \tag{19}$$

However, since $d\phi^p/d\delta$ vanishes as $\delta \to \delta_r$, the first term will inevitably be positive as slip approaches the residual value. The first term in equation (18) also tends to reduce the coefficient of $\dot{\delta}$ on the left-hand side of equation (4).

[39] The importance of fluid exchange and slow slip in the occurrence of this instability can also be deduced. If the slip rate is large, the first term on the right-hand side of equation (18) dominates the second and the response is essentially undrained. In the slow slip regime, conditions remain nearly drained, and thus $\dot{p}$ must be small. Therefore the two terms on the right-hand side of equation (18) are comparable in size.

[40] Because both the denominator $D(T(\Delta), \Delta)$ and numerator $N(\Pi, \Theta)$ of equation (9a) vanish at instability in the slow slip regime, the slip rate is indefinite at this value of slip. Consequently, the solution is not unique beyond this point. The structure of the solution near this point (described in more detail in Appendix B) suggests that an infinite multitude of slip solutions exists beyond the critical slip but that each solution of this multitude is a member of one of two families. One family evolves toward slip with an unbounded rate; the other to slip with a zero rate. Infinitesimally small slip perturbations past (but close to) the critical slip may alter the solution from one to the other family. The physical implications of this result and some improvements in the model that may alter it are discussed in section 7.

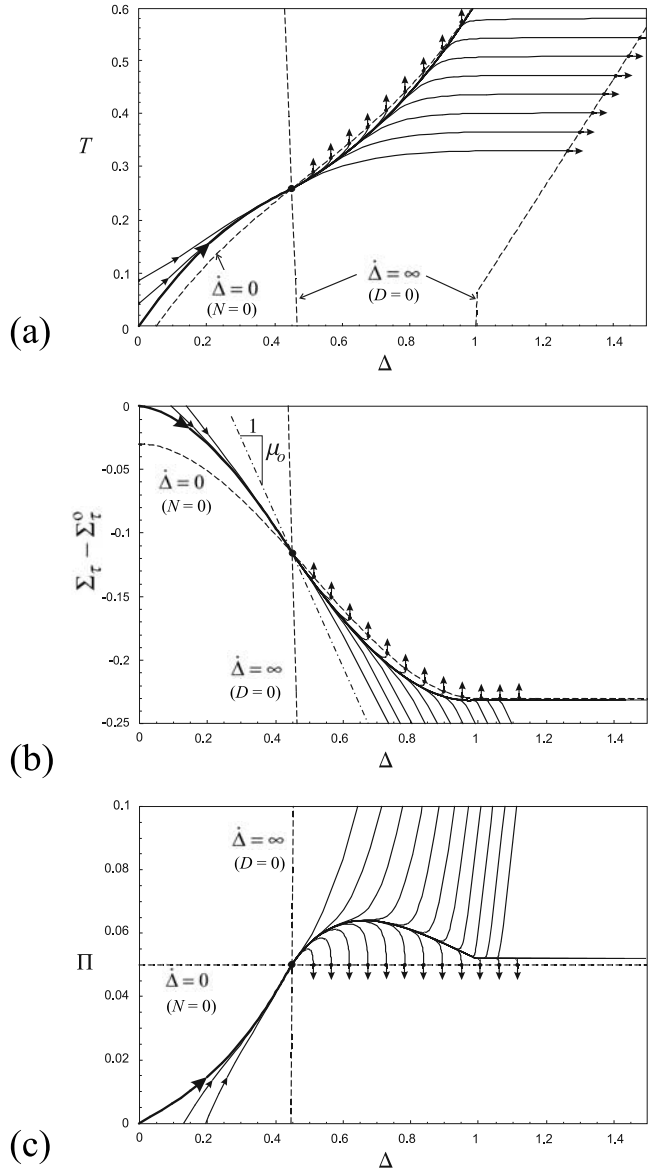

Figure 10. Illustration of loss-of-uniqueness instability in the fully drained regime for $\mathcal{A} = 0.5$, $\Phi = 0.5$, $\mathcal{B} = 0.1185$, $\Sigma_\tau^o = 9$, and $\mu_o = 0.6$ for (a) time T, (b) shear stress change, $\Sigma_\tau - \Sigma_\tau^o$, and pressure change Π versus slip Δ. (The value of drainage parameter has been taken sufficiently large, $\epsilon = 0.05$, in order to "zoom" into the solution details near and past the instability, and thermal diffusion has been neglected by comparison with pore fluid diffusion, $\epsilon_\chi \gg \epsilon$). The lines corresponding to the zero and infinite slip rate are shown dashed, and the loss-of-uniqueness state is indicated by the solid dot.

[41] Figures 10a, 10b, and 10c show a numerical example of the variation of time T, shear stress change $\Sigma_\tau - \Sigma_\tau^o$, and

pressure change Π, respectively, with slip Δ in the fully drained regime for the loss-of-uniqueness instability. An artificially large value of the drainage parameter, $\epsilon = 0.05$, was used in order to show clearly details of the solution near and past the instability. The calculation in the example also assumes that temperature diffusion is much slower than pore fluid diffusion, $\epsilon_\chi \gg \epsilon$. The instability point is shown by the dot on Figure 10 corresponding to the intersection of the two dashed lines indicating the zero and infinite slip rate, respectively). The unique and stable solution prior to the instability is shown by the thick line; the perturbed solution trajectories (thin lines prior to the instability) are shown to converge toward this solution. Past the instability point, the solution is sensitive to perturbations and evolves to either stick (the multitude of solution trajectories intersecting the $\dot{\Delta} = 0$ line) or inertial instability (the multitude of solution trajectories intersecting the $\dot{\Delta} = \infty$ line) (see Figure 10a). As discussed above, Figure 10c shows an increase of pressure due to shear heating as the instability point is approached. At the loss-of-uniqueness instability, the dimensionless slope of the effective shear stress versus slip curve exceeds the slope of the elastic unloading curve, $d\Sigma_\tau/d\Delta = -\mu_o$, (see dash-dotted line on Figure 10b). Past the instability, the solution modes evolving to stick correspond to the decreasing pore pressure and increasing shear stress; and the solution modes evolving toward the inertial instability have the opposite behavior with the slope of the effective shear stress versus slip behavior evolving toward the value at instability $-\mu_o$ (outside of the stress range shown in Figure 10b).

[42] Very qualitatively, the elevation of pore pressure by shear heating and the effect of fluid mass exchange on the slip evolution result in a diffusion-controlled process that drives the solution to the point of loss of uniqueness. This is illustrated by the converging perturbed solutions shown in Figure 10. After the instability (loss of uniqueness) point, the effective diffusion coefficient becomes negative and, as a consequence, solutions are extremely sensitive to perturbations.

6. Parametric Dependence

[43] The identification of precise criteria for stability and for instability by unbounded slip rate or by loss of uniqueness make it possible a complete evaluation of the combinations of material parameters that give rise to these various possibilities. Given the uncertainty about the appropriate values in situ for this model and, more generally, uncertainty about material and transport properties in midcrustal regions, this evaluation is essential for assessing the conditions for which these possibilities might occur in the earth.

6.1. General Observations

[44] The dependence of the slip instability criteria on the weakening $\mathcal{A}$ and dilatancy Φ, for various fixed sets of the other problem parameters, is revealed by studying the conditions for the existence of a positive root of equation (17) with equation (15). First, note that the value of the slip at instability is always in the interval $0 < \Delta_{ins} \leq 1$. When $\Delta > 1$, the derivative $dD(T_o(\Delta), \Delta)/d\Delta$ is either zero (if Δ belongs to the fully drained part of the solution) or the positive constant $\mu_o\mathcal{B}$ (if Δ belongs to the fast slip part of the asymptotic solution, i.e., when $1 < \Delta < \Delta_{**}$ and $\Delta_{**}(\mathcal{A}) > 1$, $\mathcal{A} > 4/3$). Thus $D(T_o(\Delta), \Delta)$ cannot vanish for $\Delta > 1$ unless it has already done so for $\Delta \leq 1$. Physically, the latter implies that no slip instability under nearly drained conditions can occur for $\delta > \delta_r$ when the effects of fault dilatancy and slip weakening vanish.

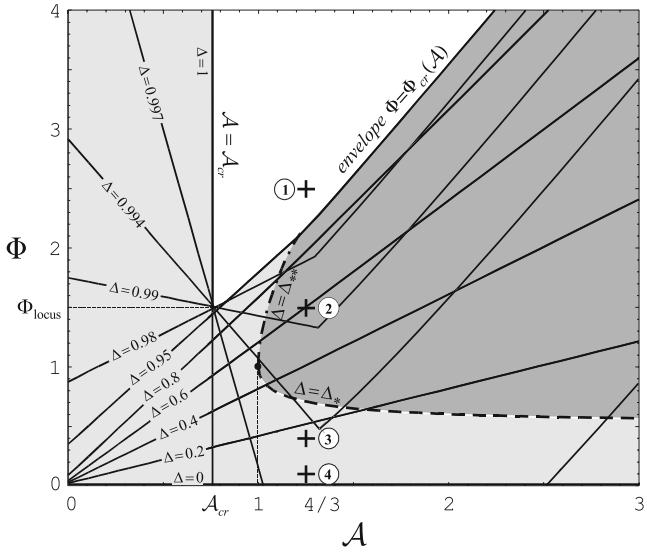

Figure 11. Contour lines of Δ_{ins} delineating the values of weakening $\mathcal{A}$ and dilatancy Φ (for fixed $\mathcal{B} = 0.115$, $\Sigma_\tau^o = 9$ and $\mu_o = 0.6$) for which slip is unstable. The domain of stable slip is shown in white; the two domains of unstable slip corresponding to the unbounded slip rate and to the loss of slip uniqueness are shown in darker and lighter grades of grey, respectively. The boundaries between different unstable slip domains correspond to $\Delta_{ins} = \Delta_*$ (dashed line) and $\Delta_{ins} = \Delta_{**}$ (dash-dotted line). See the text for more explanation.

[45] Second, because instability occurs when equation (17) has a positive root $\Delta = \Delta_{ins}$, $0 \leq \Delta_{ins} \leq 1$, the unstable slip domain on the plane $(\mathcal{A}, \Phi)$ (with the other parameters fixed) is the area swept by the family of contour lines $D(T_o(\Delta_{ins}), \Delta_{ins}; \mathcal{A}, \Phi, ..) = 0$. For example, Figure 11 shows the set of contour lines for $\{\Delta_{ins} = 0, \Delta_{ins} = 0.2, .., \Delta_{ins} = 1\}$ and $\mathcal{B} = 0.115$, $\Sigma_\tau^o = 9$, and $\mu_o = 0.6$. Slip is stable in the unshaded area, unstable by occurrence of an unbounded slip rate in the darker shaded area and unstable by loss of uniqueness in the lighter shaded area. (Intersections of the different contour lines indicate multiple values of slip for instability for a given set of parameters but only the smallest value, which is the first to occur, is relevant.) One boundary of the stable slip region is given by the contour line $\Delta_{ins} = 1$. For fixed $\mathcal{B}$, Σ_τ^o and μ_o, this condition is independent of Φ and given by the critical slip-weakening value $\mathcal{A} = \mathcal{A}_{cr}$. The other boundary is defined by the envelope $\Phi = \Phi_{cr}(\mathcal{A})$ of the contour lines $0 \leq \Delta_{ins} < 1$, which corresponds to the locus of points where $(dD(T_o(\Delta), \Delta; \mathcal{A}, \Phi, ..)/d\Delta)_{|\Delta=\Delta_{ins}} = 0$. The unstable slip domain is subdivided by the two dashed lines $\Delta_{ins}(\mathcal{A}, \Phi, ..) = \Delta_*(\mathcal{A})$ and $\Delta_{ins}(\mathcal{A}, \Phi, ..) = \Delta_{**}(\mathcal{A})$ into the two subdomains corresponding to the instability in the fast slip regime with unbounded slip rate (darker shade) and to the instability in a

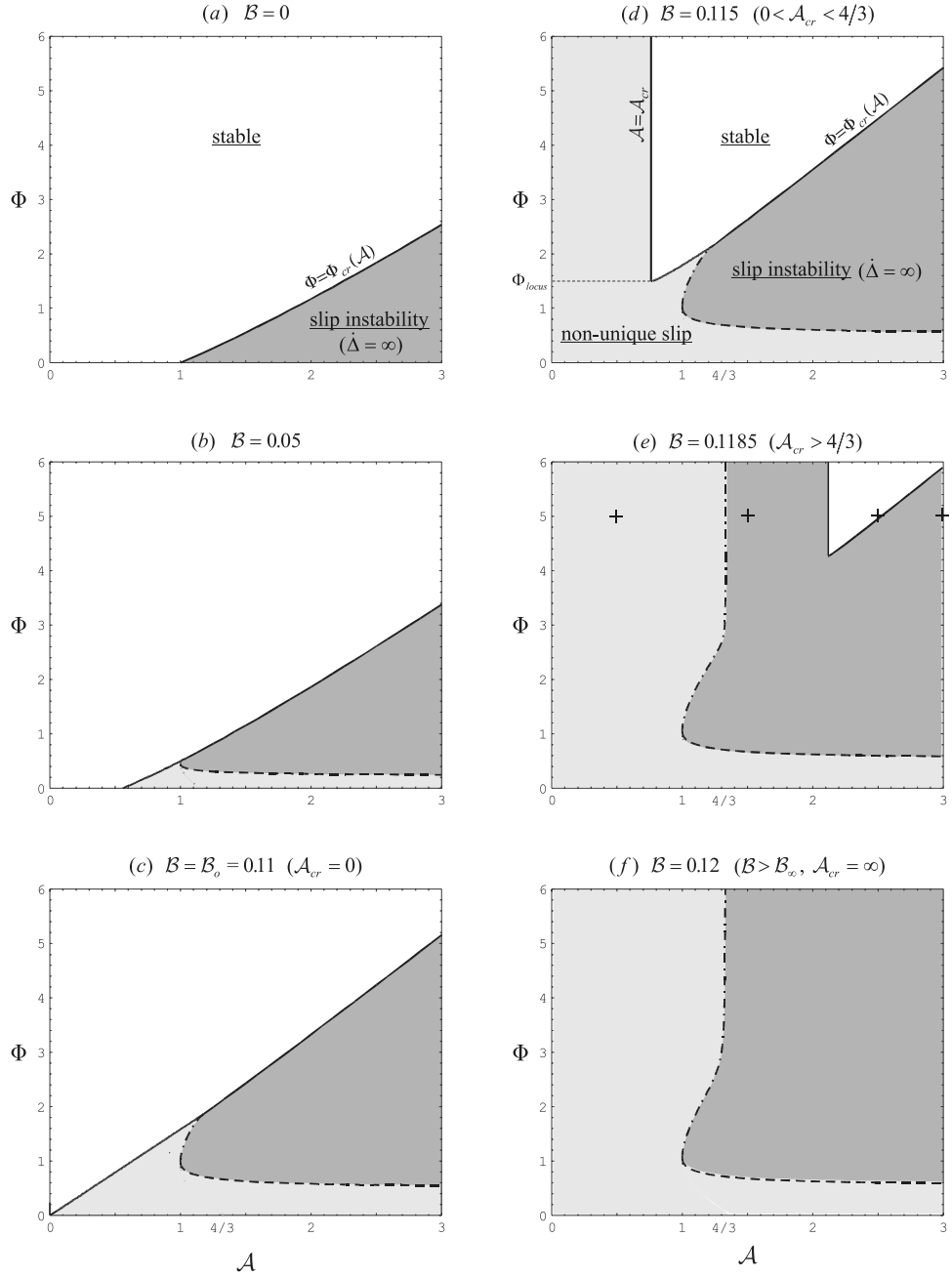

Figure 12. Stable and unstable slip domains on the parametric plane ($\mathcal{A}$, Φ) for various values of thermomechanical coupling parameter $\mathcal{B}$ and fixed $\Sigma_\tau^o = 9$ and $\mu_o = 0.6$.

fully drained regime with the loss of slip uniqueness (lighter shade).

[46] Figures 12a–12f show the evolution of domains of stable and unstable slip on the parametric plane ($\mathcal{A}$, Φ) for values of $\mathcal{B}$ increasing from $\mathcal{B} = 0$ (Figure 12a) to $\mathcal{B} = 0.12$ (Figure 12f) and fixed $\Sigma_\tau^o = 9$ and $\mu_o = 0.6$. The case in Figure 12d, $\mathcal{B} = 0.115$, is the one depicted in more detail in Figure 11. The shading is as in Figure 11.

[47] In the zero-coupling case ($\mathcal{B} = 0$) considered by RC (Figure 12a), the slip is always stable in fully drained regimes and can become unstable only in the fast slip regime ($\mathcal{A} > 1$) with the instability resulting in an unbounded slip rate. Thus slip is stable for any Φ if $\mathcal{A} < 1$ and for $\Phi > \Phi_{cr}(\mathcal{A};\ \mathcal{B} = 0) = 2(\mathcal{A} - \sqrt{\mathcal{A}})$ if $\mathcal{A} \geq 1$. The stability domain for rapid drainage, bounded by $\Phi = \Phi_{cr}(\mathcal{A};\ \mathcal{B} = 0)$, is identical to that for undrained conditions (see section 5.3 and Figure 6 of GR). This feature occurs because for zero thermomechanical coupling, the denominator D is a function of slip only and not of time.

[48] As $\mathcal{B}$ increases from $\mathcal{B} = 0$ to $\mathcal{B} = \mathcal{B}_o \equiv 1/\Sigma_\tau^o$ (Figures 12a–12c), the stability domain diminishes with its boundary shifting in the direction of larger values of dilatancy Φ and smaller values of weakening $\mathcal{A}$, reaching the $(\mathcal{A}, \Phi) = 0$ point when $\mathcal{B} = \mathcal{B}_o$ (Figure 12c). This reflects the result from GR in the limiting case of no weakening and no dilation: slip is always unstable if $\mathcal{B} > \mathcal{B}_o$. The domain corresponding to slip instability in a fully drained regime emerges as soon as $\mathcal{B}$ becomes positive (Figure 12b). Thus

the appearance of instabilities in the fully drained regime is due to the thermomechanical coupling. For small values of $\mathcal{B}$, $0 \le \mathcal{B} \le \mathcal{B}_o$, slip can be stabilized by a sufficiently large value of dilation $\Phi > \Phi_{cr}(\mathcal{A}; \mathcal{B}, \Sigma_\tau^o, \mu_o)$ for any value of frictional weakening $\mathcal{A}$; conversely, for any value of dilation, a sufficiently strong slip weakening will destabilize slip.

[49] For $\mathcal{B} > \mathcal{B}_o$ (Figures 12d and 12e), the second segment of the stability domain boundary emerges. This boundary is given by $\mathcal{A} = \mathcal{A}_{cr}(\mathcal{B}; \Sigma_\tau^o, \mu_o)$, defined implicitly by

$$\frac{1}{\mu_o}\left(\frac{1}{\mathcal{B}} - \frac{1}{\mathcal{B}_\infty}\right) = \begin{cases} 1 - \frac{2}{3}\mathcal{A}, & \mathcal{A} < 4/3 \\ T_*(\mathcal{A}), & \mathcal{A} \ge 4/3, \end{cases} \tag{20}$$

where $\mathcal{B}_\infty = (\Sigma_\tau^o - \mu_o)^{-1}$. Slip is unstable for any value of dilatancy Φ if $\mathcal{A} \le \mathcal{A}_{cr}$. Slip is also unstable for any $\mathcal{A}$ if $\Phi \le \Phi_{\text{locus}}(\mathcal{B}, \Sigma_\tau^o, \mu_o)$, where $\Phi_{\text{locus}} = \Phi_{cr}(\mathcal{A}_{cr})$ corresponds to the vertex of the stability domain boundary, i.e., the intersection of the two segments of the stability domain boundary, $\Phi = \Phi_{cr}(\mathcal{A})$ and $\mathcal{A} = \mathcal{A}_{cr}$ (see Figures 12d and 12e) and is given by

$$\Phi_{\text{locus}} = \begin{cases} 2\mathcal{A}, & \mathcal{A} < 1, \\ \max\left\{2\mathcal{A}, 4\mathcal{A}\sqrt{1 - \mathcal{A}^{-1}} + \frac{1}{2}\mu_o\mathcal{B}\right\}, & 1 \le \mathcal{A} < 4/3, \\ 2\mathcal{A} + \frac{1}{2}\mu_o\mathcal{B} & \mathcal{A} \ge 4/3. \end{cases} \tag{21}$$

For fixed $\Phi > \Phi_{\text{locus}}$, however, the stability of slip does not depend monotonically on the weakening $\mathcal{A}$. In particular, there exists an intermediate range of $\mathcal{A}$ where the slip is stable, but it is unstable for values below ($\mathcal{A} \le \mathcal{A}_{cr}$) via instability (nonuniqueness) in the fully drained regime or above this range via inertial instability in the fast slip regime. Thus increasing the slip-weakening $\mathcal{A}$ from a value below $\mathcal{A}_{cr}$ to one above $\mathcal{A}_{cr}$ stabilizes the slip. This effect can be explained along lines similar to those for the nonmonotonic dependence of the slip stability in the undrained solution on weakening $\mathcal{A}$ (see Figures 7a′–7c′ and section 5.3 of GR). Increased frictional weakening has a direct destabilizing effect but it also causes a decrease of the shear stress Σ_τ (which, according to the equilibrium equation (1), is equal to the frictional resistance) and, consequently, reduces shear heating. The reduction of shear heating has an indirect stabilizing effect. This effect is illustrated on Figure 13, where we plot the rapid drainage asymptotic solution for time, pressure and temperature versus slip for the four increasing values of weakening $\mathcal{A} = \{0.5, 1.5, 2.5, 3\}$ and a fixed value of fault dilatancy $\Phi = 5$. These values correspond to the points shown by the crosses on the $(\mathcal{A}, \Phi)$ plane on Figure 12e ($\mathcal{B} = 0.1185$, $\Sigma_\tau^o = 9$, and $\mu_o = 0.6$). Slip for $\mathcal{A} = 0.5$ is unstable in the fully drained regime (due to the loss of uniqueness); slip for $\mathcal{A} = 1.5$ and $\mathcal{A} = 3$ is unstable in the fast slip regime (due to the unbounded slip rate); and slip for the intermediate value of the weakening, $\mathcal{A} = 2.5$, is stable.

[50] The structure of the domains corresponding to the different instability types changes from Figure 12d to

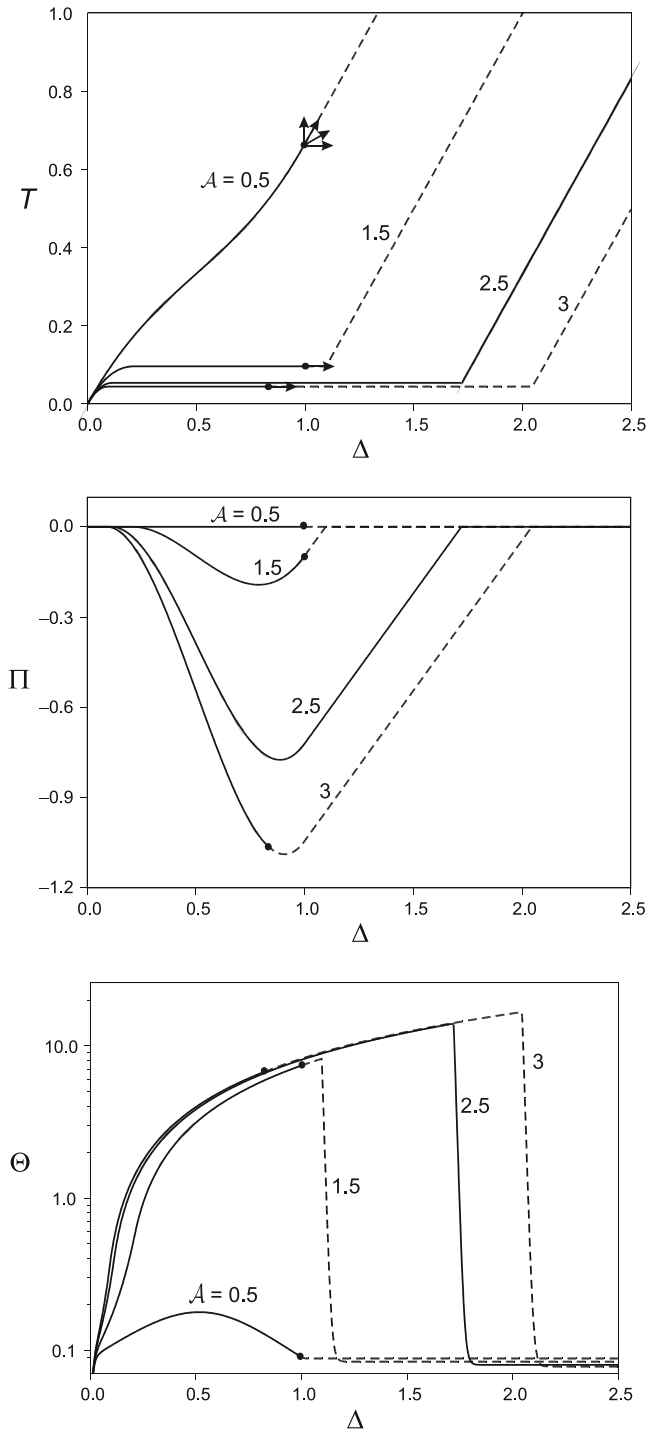

Figure 13. Dependence of slip stability on the fault weakening $\mathcal{A}$ under rapid drainage conditions (a) time T, (b) pressure Π, and (c) temperature Θ (logarithmic scale) versus slip Δ for various $\mathcal{A} = \{0.5, 1.5, 2.5, 3\}$ and fixed $\Phi = 5$, $\mathcal{B} = 0.1185$, $\Sigma_\tau^o = 9$, and $\mu_o = 0.6$. See the points shown by crosses on $(\mathcal{A}, \Phi)$ on Figure 12e. Physically meaningless parts of the slip after an instability are shown by dashed lines.

Figure 12e as $\mathcal{A}_{cr}$ passes through the value 4/3, corresponding to the value of $\mathcal{B} = 1/(\Sigma_\tau^o - \frac{8}{9}\mu_o)$. According to equation (20) and the expression for T_* ($\mathcal{A}$) (see equation (A2) of GR), $\mathcal{A} = \mathcal{A}_{cr}(\mathcal{B};\Sigma_\tau^o, \mu_o)$ is an increasing function of $\mathcal{B}$ (and Σ_τ^o) and becomes unbounded at $\mathcal{B} = \mathcal{B}_\infty$, corresponding to T_* (∞) = 0 (equation (20)). Therefore, for $\mathcal{B} \geq \mathcal{B}_\infty = 0.119$ (Figure 12f), $\mathcal{A}_{cr} = \infty$, and slip is unstable for any Φ and $\mathcal{A}$. Thus, for a given initial stress level Σ_τ^o, the slip is unstable for sufficiently large values of the thermomechanical coupling parameter $\mathcal{B}$ regardless of the dilatancy and frictional weakening on the fault; conversely for a given $\mathcal{B}$, slip is unconditionally unstable for large enough initial stress Σ_τ^o Consequently, the condition

$$\mathcal{B} \geq \mathcal{B}_\infty \equiv \frac{1}{\Sigma_\tau^o - \mu_o} \tag{22}$$

is sufficient for instability in the drained case ($\epsilon \ll 1$).

[51] Recall that a condition identical to equation (22) was sufficient for instability in the undrained ($\epsilon \gg 1$), adiabatic ($\epsilon_\chi \gg 1$) case in equations (50) and (51) of GR. In the undrained, adiabatic case, instability always occurs as an unbounded slip rate, but in the rapid drainage case, instability can correspond to loss of uniqueness or an unbounded slip rate. Nevertheless, if the stability of the slip solution is assumed to evolve monotonically with the drainage parameter ϵ from the drained to the undrained limit, then it is likely that equation (22) is a sufficient condition for instability for arbitrary drainage conditions (any $\epsilon > 0$). This conjecture that stability depends monotonically on drainage does, however, require investigation; *Chambon and Rudnicki* [2001] give an example for a rate- and state-dependent friction relation in which stability does not depend monotonically on a drainage parameter.

6.2. Depth Dependence

[52] As noted in GR, a significant feature of including shear heating is the introduction of a dependence on the absolute stress level, rather than only the stress drop. The variation of the stress level with depth introduces depth dependence into the results even if the material and transport properties are assumed to be uniform with depth. The depth dependence of the initial shear stress Σ_τ^o was estimated in section 4 of GR and for the typical material parameters set is given by (equation (35) of GR)

$$\Sigma_\tau^o = 2 + 2.4d, \tag{23}$$

where d is the depth in kilometers. Material properties, such as stress drop, porosity, and the friction coefficient, will, in general, also depend on temperature and pressure and, hence, vary with depth. Following GR, here we have included only the depth dependence of the thermomechanical coupling coefficient $\mathcal{B}$ due to variation of the pore fluid thermal expansivity β_f (since $1/K_f$ is typically negligible in the expression for K' equation (6) of GR and $K' \approx K$). For the parameters discussed in section 4 of GR, $\mathcal{B} = 20\ \theta_*\ \beta_f$ (equation (36)) and the variation of β_f with depth is shown in Figure 3 of GR. The characteristic temperature of the fault θ_* depends on the product of the fault thickness and the volumetric heat capacity, among the other parameters, and is taken at a plausible value, $\theta_* = 3.3°C$ (corresponding to the initial thickness of the fault gouge zone, $\lambda_o = 5$ cm).

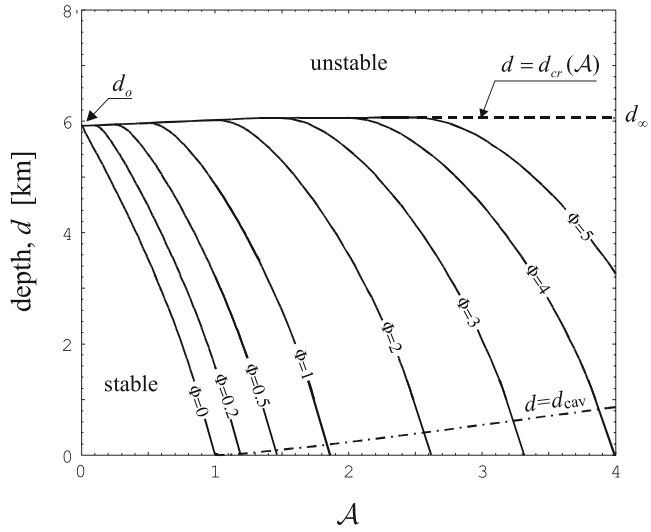

Figure 14. Dependence of slip stability on the depth d and the frictional weakening $\mathcal{A}$ for values of dilatancy Φ varying from $\Phi = 0$ to $\Phi = \infty$. Slip instability due to the shear heating and frictional weakening takes place at depths greater than indicated by the corresponding (solid) line of constant Φ. (The dashed line indicates the limit of this stability boundary when $\Phi \to \infty$.) Slip instability due to the pore fluid cavitation takes place at depths shallower than $d_{cav}(\mathcal{A})$ (dash-dotted line).

[53] Figure 14 shows the dependence of the stability domain boundary on the depth (in kilometers) d and the frictional weakening $\mathcal{A}$ for values of dilatancy Φ varying from $\Phi = 0$ to $\Phi = \infty$ and fixed $\mu_o = 0.6$. For a fixed depth of the slip the stable range of weakening $\mathcal{A}$ expands with the increase in dilation Φ. The limiting depth for stable slip $d = d_{cr}(\mathcal{A}; \mu_o)$, corresponding to $\Phi \to \infty$, is defined from $\mathcal{B}(d) = \mathcal{B}_{cr}(\mathcal{A}; \Sigma_\tau^o(d), \mu_o)$. Figure 14 shows that drained slip at depths below $d_{cr}(\mathcal{A}; \mu_o)$ is unstable for any value of dilatancy Φ and at depths below $d_\infty \simeq 6.08$ km is unstable for any Φ and $\mathcal{A}$. Because $d_{cr}(\mathcal{A}; \mu_o)$ varies between d_o (at $\mathcal{A} = 0$) and d_∞ (at $\mathcal{A} = \infty$) with $d_o \simeq 5.91$ km and $d_\infty \simeq 6.08$ km, the dependence on $\mathcal{A}$ is slight and d_{cr} is nearly a constant at a 6 km value for the choice of parameters. Interestingly, for the depth of slip between d_o and d_∞, slip is unstable for both large and small enough values of slip-weakening $\mathcal{A}$, while stable in the intermediate range. This is consistent with the nonmonotonic dependence of the slip stability on the weakening discussed in the section on general parametric dependence above. These results indicate that the critical depth below which the slip always undergoes inertial instability is bounded by approximately a 6 km value, which is fixed by the given lithostatic stress gradient and value of friction coefficient $\mu_o = 0.6$ and is approximately independent of dilatancy and stress drop on the fault.

[54] Figure 14 also shows the limiting depth at which pore pressure reductions due to dilatancy are calculated to cause cavitation of the pore fluid, $d = d_{cav}$ ($\mathcal{A}$). As noted by RC, decrease of pore fluid pressure to near the value for cavitation causes a sharp drop in the pore fluid bulk

modulus K_f and a loss of stabilization. Consequently, even if the value of dilatancy is sufficient to stabilize slip, stabilization is not possible if the ambient pore pressure is not large enough. According to the structure of the rapid drainage ($\epsilon \ll 1$) solution (15) and the expression for the pressure (equation (12a)), the pore fluid pressure p is equal (to the order ϵ) to its original value p_o except during the fast slip portion of the slip (when $\mathcal{A} > 1$) (see, for example, Figure 6a). The pressure drop in the fast slip regime (equation (A4)) reaches its maximum at $\Delta = \frac{1}{2}[1 + (1 - 1/\mathcal{A})^{1/2}] < 1$ and the corresponding minimum pressure is given by the same expression derived in RC:

$$p_{\min} = p_o - \frac{2}{3}\mathcal{A}\left(1 - \frac{1}{\mathcal{A}}\right)^{3/2} p_*, \tag{24}$$

where p_* is the characteristic pressure (or stress) in the fault gouge zone (equation (20) of GR). For the temperature range representative of the shallow crust, the cavitation pressure is very well approximated by zero. In addition, the pore fluid bulk modulus is nearly constant until the pressure approaches zero and then drops abruptly as cavitation occurs. Thus setting $p_{\min} = 0$ in equation (24) gives a good approximation for the minimum initial ambient pressure p_o that will prevent cavitation. Assuming the ambient pressure to vary with depth along the hydrostatic gradient, $p_o \approx 10d$ [MPa] and the characteristic pressure in the fault gouge zone $p_* = 5$ MPa (section 4 of GR) yields the maximum depth $d_{cav}(\mathcal{A})$ at which cavitation is predicted to occur. As shown by the dash-dotted line on Figure 14, this depth is expected to be quite shallow.

7. Discussion

[55] We have continued the investigation of the effect of shear heating on the stability of slip in GR. That paper examined the limiting cases of fully drained slip (no change of pore pressure in the fault zone), slip in the absence of weakening ($\mathcal{A} = 0$) and dilatancy ($\Phi = 0$), and undrained, adiabatic slip (no flux of fluid mass or heat from the fault zone). This paper studies the effect of shear heating on the stability of slip under nearly drained conditions, characteristic of in situ conditions when imposed loading (tectonic) rates are much slower than the rate of pore fluid exchange between the fault zone and the crustal rock. We have found (consistently with the earlier analysis in the thermally uncoupled case by RC) that when the slip weakening is smaller than the critical value, $\mathcal{A} < 1$, the fully drained solution, characterized by a slip rate of the order of magnitude of the imposed "slow" tectonic shearing rate, applies. For larger slip weakening, $\mathcal{A} \geq 1$, the fully drained solution is a good approximation over most of the slip history, but is interrupted by a period of rapid slip which can culminate in an inertial instability (unbounded slip rate corresponding to a seismic event).

[56] As expected, the occurrence of an inertial instability is, in general, enhanced by more rapid slip weakening and increased shear heating and is inhibited by increased dilation. Increased shear heating tends to increase the fault zone pore pressure, reduce the effective compressive stress and, thus the shear resistance. Increased dilation tends to reduce the pore pressure and have the opposite effect. However, as for the limiting case of undrained adiabatic response considered in GR, we also find more subtle and less expected effects. In particular, there exist parameter ranges where increased slip weakening can inhibit inertial instability and increased dilation can promote inertial instability. These effects result from their interaction with shear heating: rapid slip weakening can decrease the rate of shear heating by decreasing the shear stress; increased dilation increases the effective compressive stress and, hence, the shear resistance, which, in turn, increases the shear heating.

[57] The analysis also identifies a second type of instability that does not occur in any of the cases considered by GR. This instability occurs only in the fully drained slip regime characterized by a slow slip rate of the order of the imposed tectonic rate. This instability is not necessarily inertial but corresponds to a loss of uniqueness at which the expression for the slip rate becomes indeterminate. Although it is not possible to determine if one, or any, of the solutions beyond this point is appropriate, it is possible to show that all of them must be one of two types: those leading to zero slip rate ("stick") or those leading to unbounded slip rate.

[58] Loss of uniqueness in a model of a physical process may have a variety of interpretations. It may indicate that the model of a physical process is ill-posed, but may also indicate a change in the mode of deformation that is physically relevant: For example, buckling of a thin elastic column or the appearance of a shear band in a homogeneously deforming material are two examples. In these examples, the imperfections or inhomogeneities that exist in any real material cause the buckled mode or the shear band solution to be the one observed. In contrast to the examples just cited, the nonuniqueness here leads to one of two dramatically different states without indication of whether one or the other is preferred. Physically, this implies an extreme sensitivity to perturbations.

[59] There have been suggestions, often based on simple models, that the problem of earthquake occurrence is inherently nonpredictable and "complex". Although there could be several reasons for the appearance of nonuniqueness in the present model (one of which is discussed below), we regard the most likely explanation is an oversimplified fault slip constitutive relation. In the simple slip-weakening model the shear stress depends only on the slip and not on the rate of slip or the past history of sliding. Consequently, the fault stress is strongly constrained in the way it can adjust to altered conditions. In particular, as noted by *Segall and Rice* [1995], when rate- and state-dependent effects are included, it is not possible to separate the frictional resistance into a drained component and a time-varying effective stress.

[60] D. Garagash (unpublished research, 2003) has investigated the effect of rate dependence in the present model by replacing $g(\delta/\delta_r)$ by $g(\delta/\delta_r) - a \ln(\dot{\delta}/\dot{\delta}_{ref})$ where a is a rate sensitivity parameter and $\dot{\delta}_{ref}$ is a reference slip rate at which rate sensitivity vanishes. For a in the range $(\epsilon \mathcal{B}/\mathcal{A}) \ll a \ll 1$, he uses a modified version of the asymptotic analysis here and numerical computations to show that rate sensitivity eliminates the loss of uniqueness in the fully drained regimes. Preliminary numerical simulations show, however, that for a range of the parameter a, the slip rate undergoes slowly decaying deceleration-

acceleration oscillations due to a small slip perturbations of the fully drained solution. These oscillations in the rate-dependent model may reflect the two modes of slip evolution (toward stick or inertial instability) past loss-of-uniqueness instability in the rate-independent model. If, however, a is sufficiently smaller than $\epsilon\mathcal{B}/\mathcal{A}$, then preliminary numerical simulations show that the slip solution is unique but unstable (evolves exponentially fast toward seismic slip rates) past the nonuniqueness point of the rate-independent model. (More thorough study, including systematic variation of parameters and perturbation analysis, is required to fully assert the general behavior of the slip in the rate-sensitive model.) Finally, provided the rate sensitivity a is small enough, instability in the fast slip regime occurs when predicted by the rate-independent model. Thus the inclusion of a small amount of rate dependence has the following consequences: (1) It removes the loss of uniqueness in the fully drained regimes but may result either in slip-rate oscillations in a range of rate-sensitivity or in inertial instability if the rate-sensitivity is below a critical value related to the drainage parameter ϵ; and (2) otherwise, it does not alter the character of the solution, including the inertial instability in the fast slip regime (in this case the slip rate is bounded but evolves exponentially fast to the seismic magnitude).

[61] Much experimental work has indicated that friction of rocks (and shear of gouge) depends not only on the rate of slip but also on the state of the surface that reflects the past history of slip. Consequently, a more thorough investigation of the instability in the slow slip regime would need to include both rate and state dependence. Since faults typically spend most of their time (interseismic period) in a slow slip regime, the clarification of this instability would be significant. The lack of uniqueness occurs when the slip rate is very slow, of the same order as the imposed tectonic rate, and consequently, predictions may be quite different for the two main categories of rate- and state-dependent relations: those that allow for frictional evolution at stationary contact and those that do not. The stability characteristics of the two types have been shown to be different when used in simple one degree-of-freedom elastic systems [*Ranjith and Rice*, 1999]. Inclusion of rate- and state-dependent effects even in the current quite simple model would require a significantly more sophisticated analysis or, more likely, direct numerical solution.

[62] Inclusion of rate dependence in the fault constitutive relation resolves the lack of uniqueness, but an alternative resolution can result from use of a more elaborate description of the pore fluid exchange between the fault and the crustal rock (and of the pore fluid diffusion in the rock). Here (as by *Rudnicki and Chen* [1988] and *Segall and Rice* [1995]), the fluid mass influx into the fault is approximated as $-\kappa\,(p - p_o)/\ell$ (Figure 1) and hence depends only on the instantaneous value of the pore pressure. In contrast, in a continuum model, the fluid mass flux is proportional to the gradient of the pore pressure. The flux at the surface of a half-space with variation of pore pressure perpendicular to the surface (assuming uniform properties) depends on the past history of the pore pressure at the surface. Inclusion of this effect alleviates the ''instantaneous'' fluid flux response to the fault pressure change and related slip indeterminacy.

[63] A case that has not been considered explicitly here or in the companion paper of GR is that of a hydraulically isolated (undrained, $\epsilon \gg 1$) but nearly isothermal ($\epsilon_\chi \ll 1$) fault. Thus the fault is hydraulically isolated from the surrounding material but exchanges heat on a timescale that is rapid compared with the timescale of tectonic straining. The solution structure is, however, similar to that of the rapid drainage solution (15). Namely, for an appropriate range of parameters the initial regime of slow undrained, fully isothermal slip gives way to the fast slip regime. In the fast slip regime, the rate of slip scales with the rapid heat exchange rate $\epsilon_\chi^{-1} \gg 1$ (similar to the rapid drainage solution where the slip rate in the fast slip regime scales with the rapid fluid exchange rate ϵ^{-1}). The fast slip regime is then followed by the secondary fully isothermal regime. Analysis of the stability of undrained nearly isothermal slip via the method of Appendix B leads to conclusions similar to the ones stated above for the rapid drainage case.

8. Conclusion

[64] Under both undrained (see section 5.3 of GR) and drained slip conditions, there exists a unique critical value of the shear stress at slip initiation Σ_τ^o above which the slip is always unstable (leads to either stick or slip instability), $\Sigma_\tau^o \geq \mu_o + \mathcal{B}^{-1}$ (see equations (50) and (51) of GR and equation (22)), regardless of the amount of dilatancy and frictional weakening on the fault. When this condition is not satisfied, the slip under undrained and/or drained conditions can be either stable or unstable depending on the fault dilatancy and frictional weakening. In contrast to the undrained, adiabatic case, an increase in dilatancy will never destabilize drained slip (although an increase in dilatancy may change the type of instability, e.g., from nonuniqueness to inertial instability). For intermediate values of $\mathcal{B}$, the dependence on the slip weakening is nonmonotonic as for undrained deformation. Depending on the value of $\mathcal{B}$, an increase of slip-weakening $\mathcal{A}$, may lead to stability from a region of loss of uniqueness (smaller values of $\mathcal{B}$, see Figure 12d) or from a region of inertial instability (larger values of $\mathcal{B}$, see Figure 12e). Except for low values of the dilatancy Φ, an increase in slip-weakening $\mathcal{A}$ leads to an instability of the inertial type.

[65] Another type of instability related to shear heating is elevation of the pore pressure to the magnitude of the least compressive stress. This would cause hydraulic fracturing on planes oblique to the fault plane (and, probably, a rapid loss of pore pressure). This condition, which has been evaluated for the undrained adiabatic slip by GR, does not occur for nearly drained conditions, where there is no mechanism for elevating the pore pressure above the ambient level in the crustal rock. On the other hand, pore pressure reduction due to dilatancy can lead to instability by causing a dramatic increase in pore fluid compressibility. The calculations for the nearly drained conditions here suggest that this is a possibility primarily at shallow slip depth where the ambient values of the pore pressure are low.

[66] The depth dependence of the stability results has been illustrated by assuming the normal stress and pore pressure vary along lithostatic and hydrostatic gradients and

that the variation of the pore fluid expansivity is that of water at the pore pressure and temperature appropriate for the depth. Assuming plausible, depth-independent values of other parameters predicts stable slip for depths of about 1–6 km. The shallow depth limit is set by pore fluid cavitation $p_{\min} \leq 0$ (equation (24)), and the deep limit by shear heating (equation (22)). This is a reasonable range though it does depend on the particular parameter values and it would be unwise to assign too much significance to these particular depths. Furthermore, the simple slip-weakening description becomes increasingly suspect at depths greater than about 6–8 km. Appropriate values of the parameters of the rate- and state-dependent models are also considerably uncertain at these depths [*Blanpied et al.*, 1995]. Further uncertainty is due to the depth distribution of pore pressure itself. *Rice* [1992] has argued that the pore pressure in the San Andreas fault zones may be high, near lithostatic, over much of the depth. If so, the shear resistance would be less and vary less strongly with depth than assumed in the illustrations here.

[67] Although the analysis of this and the companion paper of GR have revealed that shear heating introduces complexity into the stability of slip, the model is simple. Some of the effects arising from this model are easily identified and have been discussed previously: shear heating of a confined fluid raises the pore pressure and decreases the shear resistance by decreasing the effective compressive stress; dilatancy of a confined fluid decreases the pore pressure and increases the shear resistance by decreasing the effective stress; both effects are diminished by rapid flow of heat and mass from the fault zone. Despite the simplicity of the model, the analysis does, however, identify several effects that are not easily anticipated. The effects cannot be attributed to a special choice of parameters since they occur in a wide range that includes values that are reasonable for faults in situ. In particular, slip weakening can stabilize slip and dilatancy can destabilize it. Both of these effects are due to the dependence of the shear heating on the absolute level of shear stress (not just its change): slip weakening diminishes the shear stress and, hence, shear heating; dilatancy increases the shear resistance and, hence, increases shear heating. Another effect that would unlikely be anticipated without the analysis is the loss of uniqueness that occurs for nonzero values of thermomechanical coupling $\mathcal{B}$. Although this feature is likely to be modified by a more elaborate rate- and state-dependent description of friction, as noted above, the resolution may depend on the particular form of the evolution for small velocities. Furthermore, although the loss of uniqueness may be eliminated by more elaborate modeling, it may indicate that the subsequent evolution will be strongly dependent on small perturbations. Finally, in contrast to other examinations of shear heating, which have focused on effects in regimes of steady or dynamic slip, the analysis here demonstrates that shear heating can have a significant effect on stability in a regime of slow slip.

Appendix A: Equations Describing the Quasi-Drained Solution

[68] For the fully drained ("slow" slip $\dot{\Delta} \sim 1$) regime I for $T < T_*$ and $\Delta < \Delta_*$, $T = T_d(\Delta)$, $\Pi = 0$, and $\Theta = \Theta_d(\Delta)$, where

$$T_d(\Delta) = \Delta - \frac{2}{3}\mathcal{A}g(\Delta) \tag{A1}$$

$$\Theta_d(\Delta) = \int_0^{\Delta} \Sigma_{\tau d}(u) \exp\left[-\frac{T_d(\Delta) - T_d(u)}{\epsilon_\chi}\right] du, \tag{A2}$$

where $\Sigma_{\tau d}(\Delta) = \Sigma_\tau^o + \mu_o(T_d(\Delta) - \Delta)$ (equation (12a)).

[69] For the fast slip ($\dot{\Delta} \sim \epsilon^{-1}$) regime for $T \simeq T_*$ and $\Delta_* < \Delta < \Delta_{**}$, $T - T_* = \epsilon\xi_f(\Delta)$, $\Pi = \Pi_f(\Delta)$, and $\Theta = \Theta_f(\Delta)$, where

$$\xi_f(\Delta) = -\int^{\Delta} \frac{D(T_*, \Delta)}{T_d(\Delta) - T_*} d\Delta, \tag{A3}$$

$$\Pi_f(\Delta) = T_d(\Delta) - T_*, \tag{A4}$$

$$\Theta_f(\Delta) = \Theta_d(\Delta_*) + \Sigma_{\tau d}(\Delta_*)(\Delta - \Delta_*) - \frac{\mu_o}{2}(\Delta - \Delta_*)^2. \tag{A5}$$

[70] For the fully drained ($\dot{\Delta} \sim 1$) regime II for $T > T_*$ and $\Delta > \Delta_{**}$, $T = T_d(\Delta)$, $\Pi = 0$, and $\Theta = \Theta_{d2}(\Delta)$, where

$$\Theta_{d2}(\Delta) = \exp\left[-\frac{T_d(\Delta) - T_*}{\epsilon_\chi}\right]\Theta_f(\Delta_{**}) + \int_{\Delta_{**}}^{\Delta} \Sigma_{\tau d}(u) \cdot \exp\left[-\frac{T_d(\Delta) - T_d(u)}{\epsilon_\chi}\right] du. \tag{A6}$$

Appendix B: Stability Analysis of the Rapid Drainage Asymptotic Solution

[71] In this appendix we verify the stability criteria for the slip under conditions of rapid drainage ($\epsilon \ll 1$) presented in the section 5. To simplify the analysis we will consider adiabatic conditions, but the qualitative results established are fully applicable under the less restrictive assumption of "slow" heat exchange, $\epsilon/\epsilon_\chi \ll 1$. The governing equation for the slip (equation (9a)) under adiabatic conditions can be rewritten as

$$\frac{d\Delta}{dT} = -\frac{1}{\epsilon\mu_o\mathcal{B}} \frac{T - T_N(\Delta)}{T - T_D(\Delta)}, \tag{B1}$$

where the functions $T_N = T - N$ and $T_D = T + D/\mu_o\mathcal{B}$ (with $\mathcal{B} \neq 0$) can be expressed as

$$T_N = T_d(\Delta) - \epsilon \tag{B2a}$$

$$T_D = \frac{1}{\mu_o\mathcal{B}}\left(\Phi f'(\Delta) + 1 - \frac{2}{3}\mathcal{A}g'(\Delta) - \mathcal{B}(\Sigma_\tau^o - \mu_o\Delta)\right). \tag{B2b}$$

Below we describe some properties of the ordinary differential equation (B1) [*Pontriagin*, 1962; *Andronov*, 1973]. These properties can be used to analyze the solution $T = T(\Delta)$ with initial condition $T(0) = 0$ for $\epsilon \ll 1$.

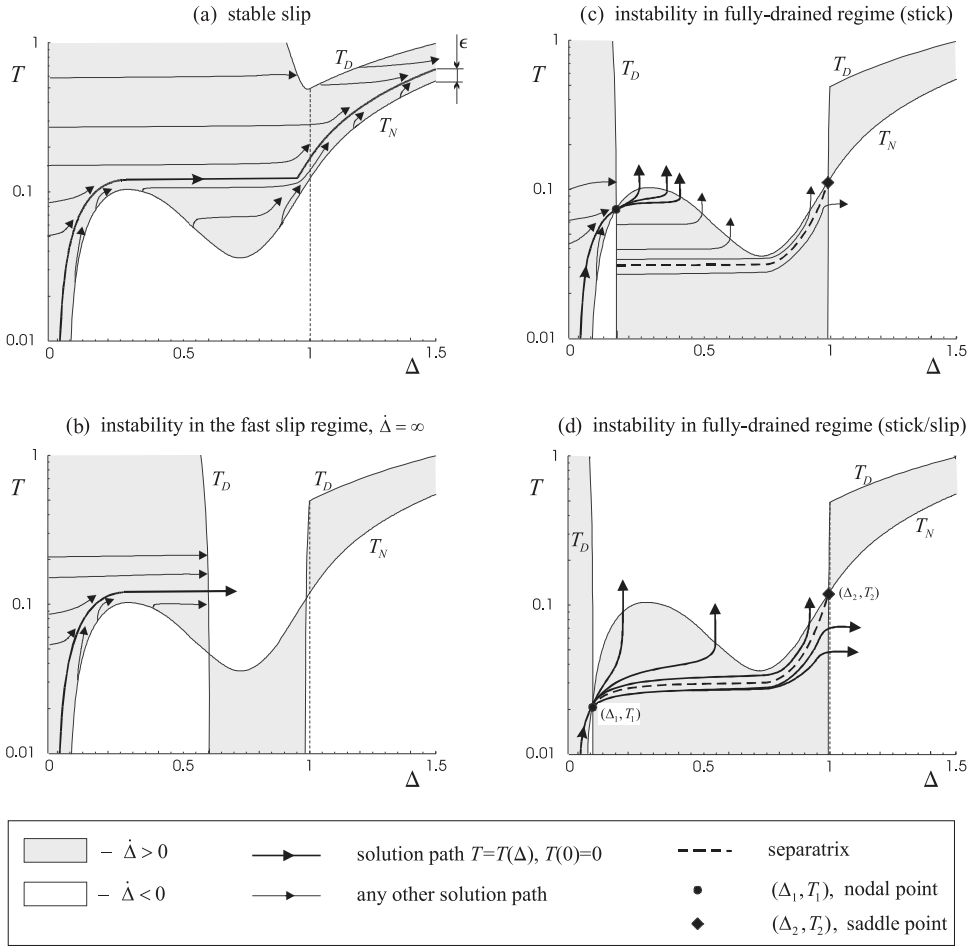

Figure B1. Analysis of the solutions $T = T(\Delta)$ (in semilogarithmic scale) corresponding to chosen points (cross marks) on the parametric plane ($\mathcal{A}$, Φ) (Figure 11). (a) Stable quasi-drained slip for $\mathcal{A} = 1.25$, $\Phi = 2.5$. Unstable slip for (b) $\mathcal{A} = 1.25$, $\Phi = 1.5$ (slip instability in the fast slip regime corresponding to the unbounded slip rate), (c) $\mathcal{A} = 1.25$, $\Phi = 0.4$ ("stick" ($\dot{\Delta} = 0$) instability), and (d) $\mathcal{A} = 1.25$, $\Phi = 0.1$ ("stick-slip" instability). (The value of ϵ (scaling the offset between the stable part of the solution in a fully drained regime and isocline $T = T_N(\Delta)$) is exaggerated for the clarity.)

[72] Possible solutions of the ODE (equation (B1)) can be viewed as curves in the (Δ, T) plane, and the vector field ($\dot{\Delta}$, 1) is tangent to those curves. On the special curves, called critical isoclines $T = T_N(\Delta)$ and $T = T_D(\Delta)$, the vector ($\dot{\Delta}$, 1) is vertical and horizontal, respectively. Consequently, any solution path which intersects one of the two isoclines $T = T_N(\Delta)$ or $T = T_D(\Delta)$ yields zero or infinite slip rate, respectively. The points of intersection of the two critical isoclines (if they exist) are called special points of the ODE (equation (B1)) and are characterized by an indefinite slip rate. Consequently, if any solution path goes through a special point it becomes nonunique, i.e., multiple solution paths are possible past this special point. The area on the (Δ, T) plane between the two critical isoclines, $T_N \leq T \leq T_D$, corresponds to positive slip rate. The inclination of the vector field ($\dot{\Delta}$, 1) is nearly horizontal, i.e., slip rate is large, $\dot{\Delta} \sim 1/\epsilon \gg 1$ (B1), everywhere on the (Δ, T) plane except for the ϵ vicinity of the isocline $T = T_N(\Delta)$. In this vicinity the slip rate varies between zero on the isocline to large values, $\dot{\Delta} \gg 1$, at the distances more than ϵ away from the isocline.

[73] The isocline $T = T_N(\Delta)$ (equation (B2a)) is positioned ϵ below the fully drained curve $T = T_d(\Delta)$. For the form of the functions f and g adopted in equations (6) and (8), the isocline $T = T_D(\Delta)$ is parabolic for $\Delta < 1$ and linear, $T_D'(\Delta) = 1$, for $\Delta \geq 1$. Because of the f'' discontinuity at $\Delta = 1$, the slope of $T = T_D(\Delta)$ is discontinuous there. Figure B1 depicts qualitative plots of the isoclines in a semilogarithmic scale for different choices of parameters Φ and $\mathcal{A}$ (The negative parts of isoclines, where applicable, are not shown.) For clarity, a value of ϵ much larger than the estimate $\epsilon \sim 10^{-10}$ to 10^{-6} provided in GR (equation (34)) was used in the above plots.

B1. Stable Slip (Unique Slip Solution With Bounded Slip Rate)

[74] The slip solution $T = T(\Delta)$ with $T(0) = 0$ is stable (i.e., the slip rate is bounded and the solution is stable with respect to small perturbations) and is given to the order ϵ by the asymptotic $\epsilon \ll 1$ solution (equation (15)), $T = T_o(\Delta) + O(\epsilon)$, if and only if $T_D(\Delta) > T_o(\Delta)$ for all Δ, or, equiva-

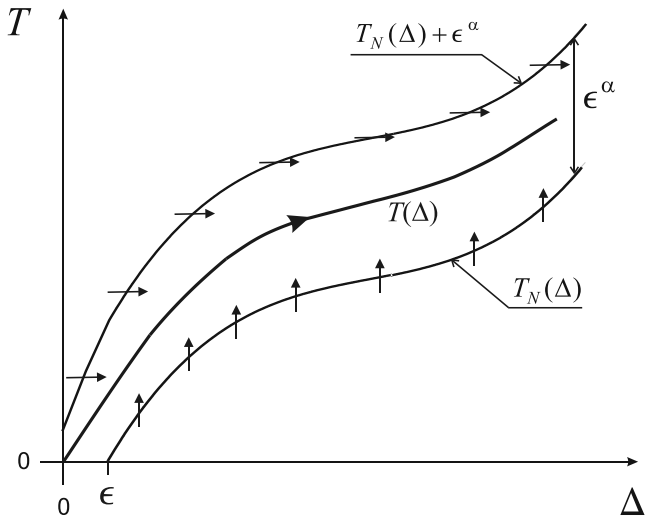

Figure B2. Sketch of the (ϵ^{α})-neighborhood ($0 < \alpha < 1$) of the vertical isocline $T = T_N(\Delta)$.

lently, $D(T_o(\Delta), \Delta) > 0$ for any Δ. (This inequality has to be understood to the order ϵ, i.e., $(T_D(\Delta) - T_o(\Delta))/T_o(\Delta) \gg \epsilon$ for any Δ.) The stability criterion implies that $T_D(\Delta) > T_N(\Delta)$ since $T_N(\Delta)$ is smaller than $T_o(\Delta)$ by at least ϵ, and therefore no special points (intersections of the critical isoclines) exist in this case.

[75] To verify the above criterion, first consider the case $\mathcal{A} < 1$ (i.e., $T_N'(\Delta) > 0$ for all Δ) and $T_D(\Delta) > T_N(\Delta)$. Let us select the ($\epsilon^{\alpha}$)-plus neighborhood of the vertical isocline, $0 < T - T_N(\Delta) < \epsilon^{\alpha} \ll 1$ with $0 < \alpha < 1$. Then, according to the properties of the tangential vector field of equation (B1), the inclination of the vector field is nearly horizontal ($\dot{\Delta} \sim \epsilon^{\alpha-1} \gg 1$) on the upper boundary of the neighborhood, $T = T_N(\Delta) + \epsilon^{\alpha}$, and is vertical ($\dot{\Delta} = 0$) on the lower boundary, $T = T_N(\Delta)$. Consequently, no solution path which is initiated inside the neighborhood can leave it (all solution paths crossing the boundary of the neighborhood are incoming); see the sketch on Figure B2.

[76] The slip initiation point for the solution of interest is at the origin, $T(0) = 0$, and is inside the neighborhood. Therefore the solution $T = T(\Delta)$ has to remain in the ϵ plus neighborhood of $T = T_N(\Delta)$ for all Δ and thus is given by the fully drained solution to the order ϵ.

[77] In the case $\mathcal{A} \geq 1$, characterized by nonmonotonic $T_N(\Delta)$, the solution $T = T(\Delta)$ remains in the ϵ plus neighborhood of $T = T_N(\Delta)$ for $\Delta < \Delta_*$, from where it then departs to form a nearly horizontal line for $\Delta > \Delta_*$ (tangential vector field is nearly horizontal away from the isocline $T = T_N(\Delta)$) and, finally, reenters the ϵ plus neighborhood of $T = T_N(\Delta)$ in the vicinity of $\Delta = \Delta_{**}$ to remain there for $\Delta > \Delta_{**}$; see, for example, Figure B1a. Parameters for the depicted case of stable slip correspond to the point 1 on the parametric plane ($\mathcal{A}$, Φ) of Figure 11.

B2. Unstable Slip

[78] Slip is unstable when there exists a slip value Δ_{ins}, such that $D(T_o(\Delta_{\text{ins}}), \Delta_{\text{ins}}) = 0$, or $T_D(\Delta_{\text{ins}}) = T_o(\Delta_{\text{ins}})$.

B2.1. Instability in the Fast Slip Regime

[79] Slip instability in the fast slip regime, $\Delta_{\text{ins}} \in (\Delta_*, \Delta_{**})$, $T_D(\Delta_{\text{ins}}) = T_*$, corresponds to the unbounded slip rate $\dot{\Delta} = \infty$. Indeed, in this case the exact solution $T = T(\Delta)$ approximated by the asymptotic solution, $T = T_o + O(\epsilon)$, intersects the critical isocline $T = T_D(\Delta)$ away from the other critical isocline $T = T_N(\Delta)$ (since $T_N(\Delta) < T_*$ for $\Delta \in (\Delta_*, \Delta_{**})$) (see Figure B1b), yielding infinite slip rate. Parameters for the depicted case correspond to the point 2 on the parametric plane ($\mathcal{A}$, Φ) of Figure 11.

B2.2. Nonunique Slip

[80] Slip instability in a fully drained regime, $\Delta_{\text{ins}} \in (0, \infty) \backslash (\Delta_*, \Delta_{**})$, $T_D(\Delta_{\text{ins}}) = T_d(\Delta_{\text{ins}})$ corresponds to the loss of slip uniqueness and subsequent instability with respect to a small perturbation. To demonstrate that, proceed with the following analysis.

[81] Since $T = T_d(\Delta)$ is ϵ close to the critical isocline $T = T_N(\Delta)$, then the above instability condition in a fully drained regime implies that the two critical isoclines intersect at the special point (Δ_1, T_1), $T_D(\Delta_1) = T_N(\Delta_1) = T_1$, where the slip value at the special point is approximated by Δ_{ins}, i.e., $\Delta_1 = \Delta_{\text{ins}} + O(\epsilon)$. (Note that given the parabolic shape of the isocline $T = T_D(\Delta)$, the second special point (Δ_2, T_2) may exist past the first one). To understand behavior of a slip solution in the vicinity of a special point, we consider the eigenproperties of the ODE (equation (B1)) Jacobian evaluated at the special point

$$J(\Delta) = \begin{pmatrix} -T_N'(\Delta) & 1 \\ \bar{\epsilon} T_D'(\Delta) & -\bar{\epsilon} \end{pmatrix}, \qquad \bar{\epsilon} = \epsilon \mu_o \mathcal{B} \ll 1. \tag{B3}$$

Eigenvalues $\lambda_{\text{I,II}}$ and corresponding eigenvectors $\mathbf{e}_{\text{I,II}}$ of $J(\Delta)$ are

$$\lambda_{\mathbf{I}} = -T_N' - \bar{\epsilon}\frac{T_D'}{T_N'}, \quad \lambda_{\mathbf{II}} = \bar{\epsilon}\frac{T_D' - T_N'}{T_N'}, \quad \mathbf{e}_{\text{I,II}} = \left\{1, T_N' + \lambda_{\text{I,II}}\right\}, \tag{B4}$$

where the higher-order $\bar{\epsilon}$ terms have been neglected. Thus the eigenvalues are of the same sign, $\lambda_{\text{I}}\lambda_{\text{II}} > 0$, at the first special point (Δ_1, T_1) with $T_D' < T_N'$, and of the opposite sign, $\lambda_{\text{I}}\lambda_{\text{II}} < 0$, at the second special point (Δ_2, T_2) with $T_D' > T_N'$. According to the classical ODE theory [*Pontriagin*, 1962], (Δ_1, T_1) is then the nodal point (all solution paths in the vicinity of the ODE nodal point are incoming to or outgoing from the point) and (Δ_2, T_2) is the saddle point (only two limiting solution paths, called separatrices, pass through the point). Thus the solution path $T = T(\Delta)$ with the initial condition $T(0) = 0$ passes through the nodal point (Δ_1, T_1) and becomes nonunique, such that additional information (refinement of the model) is needed to single out the solution path past the nodal point. Note that all solution paths exiting the nodal point (which can be the continuation of the solution path $T = T(\Delta)$, $T(0) = 0$, past the nodal point) have identical slope defined by the second eigenvector, $\mathbf{e}_{\text{II}} = \{1, T_N' + \lambda_{\text{II}}\}$ (equation (B4)) (since $-\lambda_{\text{II}} \sim \bar{\epsilon}$, this slope is slightly (by $\bar{\epsilon}$) smaller than the slope of the critical isocline $T = T_N(\Delta)$).

[82] Loss of solution uniqueness at the nodal special point is shown on Figures B2c and B2d for two different sets of problem parameters corresponding to the points 3

and 4 on the parametric plane $(\mathcal{A},\Phi)$ of Figure 11. Solution path $T = T(\Delta)$ with $T(0) = 0$ is shown by the thick line. Evolution of the multitude of the slip solutions past the special point depends on the second special point (Δ_2, T_2). In general, one of the separatrices incoming to (Δ_2, T_2) (shown in thick dashed line) divides solution paths into two families. Any path from the first family (above the dividing separatrix) crosses the critical isocline $T = T_N(\Delta)$ at some value of slip in the interval between the nodal and saddle points, $\Delta \in (\Delta_1, \Delta_2)$, and, therefore, leads to stick ($\dot{\Delta} = 0$). Any path from the second family of solution paths (below the dividing separatrix) crosses the critical isocline $T = T_D(\Delta)$ at some $\Delta \in (\Delta_1, \Delta_2)$ and therefore leads to the slip instability with the unbounded slip rate ($\dot{\Delta} = \infty$). Since all solution paths (including the separatrix) of the ODE (equation (B1)) are nearly horizontal on (Δ, T) plane away from the critical isocline $T = T_N(\Delta)$, the separatrix connects the two special points (i.e., is outgoing from the nodal point and incoming to the saddle point) if $T_1 < \min_{\Delta_1<\Delta<\Delta_2}\{T_2, T_N(\Delta)\}$. Consider the case depicted on Figure B1c, where the above condition is not satisfied and, consequently, the separatrix lies below the line $T = T_1$. All the multitude of solution paths exiting (Δ_1, T_1) lead to stick (each solution path crosses $T = T_N(\Delta)$ and thus yields $\dot{\Delta} = 0$). On the other hand, in the case depicted on Figure B1d the above inequality is satisfied and the separatrix connects the two special points, thus, divides the multitude of solution paths exiting the nodal point (Δ_1, T_1) into the two families leading to either stick (first family) or unbounded slip rate (second family). Since all paths exiting (Δ_1, T_1) at the same angle, any infinitesimal positive (negative) slip perturbation immediately after the passage of the nodal point can result in the change of solution family, i.e., in eventual slip instability with unbounded slip rate instead of stick (and vice versa).

Notation

Material, geometry, and loading constants

- G elastic shear modulus of the crustal rock.
- κ, χ hydraulic and thermal conductivities of the rock.
- C heat capacity of the fault gouge.
- K' effective bulk modulus of the gouge.
- μ_o friction coefficient of the gouge.
- β' effective thermal expansivity of the gouge (function of the ambient pressure p_o and temperature θ_o).
- ℓ half thickness of the crustal block.
- λ_o initial half thickness of the fault zone.
- d depth of the slip.
- $p_o(d)$ ambient value of pore pressure.
- $\theta_o(d)$ ambient value of temperature.
- $\dot{\gamma}_\ell$ tectonic shear strain rate.
- τ_o initial fault shear resistance.

Slip characteristic parameters

- t_s slip timescale, equal to $\delta_r/(\dot{\gamma}_\ell \ell)$.
- t_κ pore fluid diffusion timescale, equal to $\lambda_o \ell/(\kappa K')$.
- t_χ thermal diffusion timescale, equal to $\lambda_o \ell C/\chi$.
- δ_r residual slip distance.
- τ_r residual fault shear resistance.
- ϕ_r^p residual inelastic change of porosity.
- p_* characteristic pore pressure, equal to $(G/\mu_o)(\delta_r/\ell)$.
- θ_* characteristic temperature, equal to $(p_*/C)(\delta_r/\lambda_o)$.

Dimensional and normalized variables

- t and $T = t/t_s$ time.
- δ and $\Delta = \delta/\delta_r$ fault slip.
- τ and $\Sigma_\tau = \tau/p_*$ shear stress on the fault.
- $p - p_o$ and $\Pi = (p - p_o)/p_*$ pore pressure variation (in the fault zone).
- $\theta - \theta_o$ and $\Theta = (\theta - \theta_o)/\theta_*$ temperature variation (in the fault zone).

Governing dimensionless parameters and functions

- ϵ pore fluid exchange parameter, equal to t_κ/t_s.
- ϵ_χ heat exchange parameter, equal to t_χ/t_s.
- $\Sigma_{\tau o}$ initial shear stress on the fault, equal to τ_o/p_*.
- $\mathcal{A}$ frictional slip weakening, equal to $\frac{3}{2}(\tau_o - \tau_r)/(\mu_o p_*)$.
- $\mathcal{B}$ thermomechanical coupling, equal to $\beta'\theta_*$ (K'/p_*).
- Φ inelastic dilation parameter, equal to $\phi_r^p(K'/p_*)$.
- $g(\Delta < 1)$ function specifying frictional stress decrease with the slip, equal to $-2\Delta^3 + 3\Delta^2$.
- $f(\Delta < 1)$ function specifying inelastic dilation of the fault with the slip, equal to $2\Delta - \Delta^2$ (with $f(\Delta \geq 1) = g(\Delta \geq 1) = 1$).

[83] **Acknowledgments.** This work was supported by the National Science Foundation under grant EAR-9526767 and the U.S. Department of Energy, Office of Basic Energy Sciences grant DE-FG02-93ER14344. Review comments of Paul Segall led to considerable improvement in the paper.

References

Andrews, D. J., A fault constitutive relation accounting for thermal pressurization of pore fluid, *J. Geophys. Res.*, *107*(B12), 2363, doi:10.1029/2002JB001942, 2002.

Andronov, A. A., *Qualitative Theory of Second-Order Dynamic Systems*, John Wiley, Hoboken, N. J., 1973.

Blanpied, M. L., and T. E. Tullis, The stability and behavior of a frictional system with a two state variable constitutive law, *Pure Appl. Geophys.*, *124*, 415–444, 1986.

Blanpied, M. L., D. A. Lockner, and J. D. Byerlee, Frictional slip of granite at hydrothermal conditions, *J. Geophys. Res.*, *100*, 13,045–13,064, 1995.

Byerlee, J., Friction, overpressure and fault normal compression, *Geophys. Res. Lett.*, *17*, 2109–2112, 1990.

Chambon, G., and J. W. Rudnicki, Effects of normal stress variations on frictional stability of a fluid-infiltrated fault, *J. Geophys. Res.*, *106*, 11,353–11,372, 2001.

Garagash, D. I., and J. W. Rudnicki, Shear heating of a fluid-saturated slip-weakening dilatant fault zone: 1. Limiting regimes, *J. Geophys. Res.*, *108*(B2), 2121, doi:10.1029/2001JB001653, 2003.

Gu, J.-C., J. R. Rice, A. L. Ruina, and S. T. Tse, Slip motion and stability of a single degree of freedom elastic system with rate and state dependent friction, *J. Mech. Phys. Solids*, *32*, 167–196, 1984.

Henyey, T. L., and G. L. Wasserburg, Heat flow near major strike-slip faults in California, *J. Geophys. Res.*, *76*, 7924–7946, 1971.

Lachenbruch, A. H., Frictional heating, fluid pressure, and the resistance to fault motion, *J. Geophys. Res.*, *85*, 6097–6112, 1980.

Lachenbruch, A. H., and J. H. Sass, Thermo-mechanical aspects of the San Andreas, in *Proceedings, Conference on the Tectonic Problems of the San Andreas Fault System*, edited by R. L. Kovach and A. Nur, *Stanford Univ. Publ. Geol. Sci.*, *13*, 192–205, 1973.

Mase, C. W., and L. Smith, Effects of frictional heating on the thermal, hydrologic, and mechanical response of a fault, *J. Geophys. Res.*, *92*, 6249–6272, 1987.

Pontriagin, L. S., *Ordinary Differential Equations*, Addison-Wesley-Longman, Reading, Mass., 1962.

Raleigh, C. B., and J. Evernden, Case for low deviatoric stress in the lithosphere, in *Mechanical Behavior of Crustal Rocks*, *Geophys. Monogr. Ser.*, vol. 24, edited by N. L. Carter et al., pp. 173–186, AGU, Washington, D. C., 1981.

Ranjith, K., and J. R. Rice, Stability of quasi-static slip in a single degree of freedom elastic system with rate and state dependent friction, *J. Mech. Phys. Solids*, *47*, 1207–1218, 1999.

Rice, J. R., Theory of precursory processes in the inception of earthquake rupture, *Gerländs Beitr. Geophys.*, *88*, 91–127, 1979.

Rice, J. R., Fault stress states, pore pressure distributions, and the weakeness of the San Andreas fault, in *Fault Mechanics and Transport Properties of Rock*: *A Festschrift in Honor of W. F. Brace*, edited by B. Evans and T.-F. Wong, pp. 475–503, Academic, San Diego, Calif., 1992.

Rice, J. R., and A. Ruina, Stability of steady frictional slipping, *J. Appl. Mech.*, *105*, 343–349, 1983.

Rice, J. R., and S. T. Tse, Dynamic motion of a single degree of freedom system following a rate and state dependent friction law, *J. Geophys. Res.*, *91*, 521–530, 1986.

Rudnicki, J. W., and C.-H. Chen, Stabilization of rapid frictional slip on a weakening fault by dilatant hardening, *J. Geophys. Res.*, *93*, 4745–4757, 1988.

Segall, P., and J. R. Rice, Dilatancy, compaction, and slip instability of a fluid-infiltrated fault, *J. Geophys. Res.*, *100*, 22,155–22,171, 1995.

Shaw, B. E., Frictional weakening and slip complexity in earthquake faults, *J. Geophys. Res.*, *100*, 18,239–18,251, 1995.

Sibson, R. H., Interaction between temperature and fluid pressure during earthquake faulting—A mechanism for partial or total stress relief, *Nature*, *243*, 66–68, 1973.

Sleep, N. H., Frictional heating and the stability of rate and state dependent frictional sliding, *Geophys. Res. Lett.*, *22*, 2785–2788, 1995.

D. I. Garagash, Department of Civil and Environmental Engineering, Clarkson University, Potsdam, NY 13699-5710, USA. (garagash@clarkson.edu)

J. W. Rudnicki, Department of Civil and Environmental Engineering, Northwestern University, Evanston, IL 60208-3109, USA. (jwrudn@northwestern.edu)